HYDROLOGICAL CONTROLS ON PSEUDOKARST IN A PERMIAN SANDSTONE SILTSTONE AQUIFER, OKLAHOMA

By

JORDON PATRICK MASSEY

Bachelor of Science in Geology

Western Michigan University

Kalamazoo, Michigan

2018

Submitted to the Faculty of the
Graduate College of the
Oklahoma State University
in partial fulfillment of
the requirements for
the Degree of
MASTER OF SCIENCE
December 2021

HYDROLOGICAL

CONTROLS ON PSEUDOKARST IN A PERMIAN

SANDSTONE SILTSTONE AQUIFER, OKLAHOMA

Thesis Approved:

Dr. Todd Halihan

Thesis Adviser

Dr. Natascha Riedinger

Dr. Javier Vilcaez

ACKNOWLEDGEMENTS

I would like to acknowledge my parents, for without their, belief, support, and love I would not have even dreamed about making it to the level I am at now. To my momma and pops, as y'all know, it took a lot of work, but we are almost there, I'll see you all in four years for the final level up!

Next, I'd like to thank my grandparents. As a child I was lucky enough to have both sets of grandparents. They taught me so much, even guided me to the path I am on now. I am doing this for you all, thank you so much!

I'd like to thank Mr. Young from EcoTek labs in Detroit, MI. If it wasn't for your program, I would not have found a successful pathway to become a researcher. Mr. Young took another student and I down to the Gulf of Mexico in 2010 to study the effects on the Deep Horizon Oil Spill. It was here where I observed the effects we have when we contaminate our environment. This trip alone changed my outlook on not only environmental safety but on my life. Thank you, Mr. Young.

I would like to thank my professors from Western Michigan University: Drs. Kominz and Kehew. Dr. Kominz and I used to meet every Friday to talk about my progress in classes. She helped me to believe in myself as a scientist, and for that I thank you so much! Dr. Kehew took me on a trip in 2017 that would change my perspective on geology. Up until this trip I only felt the power of geology once and that was when I learned about structural geology. The trip took us to the Illinois-Kentucky border, where we came upon a river channel that flooded when the nearby karst caves filled with water. I got to stand in the channel which was about 20 ft tall. I remember walking down the channel and seeing a six foot diameter tree wedged against other trees like a stick caught in a drain. For the first time in my geological career, I felt small. This started my pursuit of karst knowledge. Thank you Dr. Kehew!

I'd like to thank Dr. T, Dr. Mohamed and the BPSoG for taking a chance on a student from the mitten state. We are not done yet!

Lastly, I'd like to thank all those who have helped me think through tough situations and helped provide me with the positive energy I needed to reach this point in my academic career. A special thanks to Dionne Mayibeki, for motivating me to be better. In the next four years, I will need you all's help more than ever as I pursue a Ph.D. in Geology!

Name: Jordon Massey

Date of Degree: DECEMBER 2021

Title of Study: HYDROGEOLOGICAL CONTROLS ON PSEUDOKARST IN A PERMIAN SANDSTONE SILTSTONE AQUIFER, OKLAHOMA

Major Field: GEOLOGY

Abstract: Pseudokarst formation is a combination of both dissolution and piping processes (collectively referred to as arenization), that both contribute to the removal of subsurface mass along preferential pathways. Much of the focus of pseudokarst formation research literature has been centered around the dissolution mechanism for quartz arenite sandstone aquifers. As quartz sediment is relatively insoluble, this focus on the process of dissolution limits the understanding of pseudokarst formation by not evaluating the effects of sediment piping along preferential pathways. This study uses hydrological, geophysical and land survey data to delineate how the piping aspect of arenization through fine grained units contributes to the development of pseudokarst in a weakly bonded sandstone siltstone in Stillwater, Oklahoma. Using pressure transducers, water level and EC data were collected from groundwater and surface water locations, and demonstrated the presence of low permeability sediment slopes covering the aquifer resulting in a strong horizontal hydraulic gradient of 0.114 during storm events. Two electrical resistivity images (ERI) and one Temporal ERI (TERI) were collected across the field site. The ER data illustrated the geologic structure of a slope with significant pseudokarst development. Data from the temporal ERI delineated the location of the dominant flow path for the study area. GPS and well data were collected to quantify the location of sinkholes and elevations of lithological changes in the study site. At this field site, the water is focused along pseudokarst pipes caused by low permeability zones in the siltstone lithology, leading to the arenization of material along these preferential flow pathways. Integrated analysis of hydrological, geophysical and land survey data showed the importance of vertical permeability variations in fine grained siltstone units and clay residual controlling the flowpaths which allow dissolution and piping from the system. Contrary to current literature, these results demonstrate the importance of fine grain units and residual sediments as hydrogeologic controls of pseudokarst development.

TABLE OF CONTENTS

Chapter Page

LIST OF TABLES

Table Page

LIST OF FIGURES

CHAPTER I

1.0 INTRODUCTION

Sandstone is a common sedimentary rock which weathers based on the composition of both the primary grains and the type of cement that binds the material. Where sandstone weathers it can develop pseudokarst, or karst-like, landforms, like gullies, blind valleys, sinkholes, and caves, which can potentially lead to collapses, unpredictable contaminant transport, and hazardous infiltration of contaminants from the surface into the subsurface (Aubrecht et al., 2011; Bruthans et al., 2012; Ford et al., 2013; Mecchia et al., 2019; Sauro, 2014; Wray, 2009; Wray et al., 2017). Psuedokarst development is conceptualized as a process that combines weathering through chemical dissolution, such as karst development in carbonates, with mechanical piping of solids, such as occurs in unconsolidated soils (Wray and Sauro, 2017). To evaluate the occurrence of pseudokarst development, both processes that contribute to formation must be quantified, however most current studies only define its processes through either dissolution or piping processes rather than interpreting landscapes as the combination of both (Marco et al., 2008; Martin et al., 2001; Martin et al., 2006; Wray and Sauro, 2017). This leads to a misunderstanding when attempting to predict development of pseudokarst landscapes in aquifers containing varying lithologies. The objective of this thesis is to

identify, in a field setting, how hydrological controls of sandstone siltstone aquifers contribute to pseudokarst formation.

1.1 Karst Dissolution Controls

In consolidated aquifers containing soluble mineral species, the dissolution of the rock matrix along permeable pathways is the primary cause of karstification (Filipponi et al., 2009). Commonly, when carbon dioxide becomes diffused into the water it forms carbonic acid, which causes the dissolution of carbonate rock leading to the formations of karst landscapes (Ford and Williams, 2013). However, as the partial pressure of carbon dioxide changes in the aquifer, the rate of dissolution becomes more dependent on temperature and the speed at which ions are removed from a surface (Wray and Sauro, 2017). When thermodynamically aggressive fluids interact with lithology containing soluble mineral species, dissolution or precipitation can occur depending on the amount of solute at a given temperature, pressure, and time (Bandstra et al., 2008; Buhmann and Dreybrodt, 1985; Filipponi et al., 2009; Piccini and Mecchia, 2009; Sauro, 2014; Williams, 1983; Wray and Sauro, 2017; Zhao et al., 2009). Without a constant flux of new chemically aggressive fluids, dissolved concentrations of the rock matrix will become saturated and dissolution will cease. The long-term development and enlargement of karst conduits is directly proportional to the flux of dissolving fluids interacting with the aquifer (Douglas 1978; Wray 2017).

In soluble carbonate aquifers, inception horizons have been found to provide the constant flux necessary for karst formation. An inception horizon is the part of the rock succession that is particularly susceptible to the development (enlargement) of karst conduits due to physical, lithological, or chemical deviation from the predominate

carbonate faces within the limestone sequence (Filipponi et al., 2009). Inception horizons provide groundwater with preferential pathways through the aquifer, thus controlling how fluids cycle through the subsurface (Filipponi et al., 2009; Marco and Pierre-Yves, 2008; Sauro, 2014; Wray and Sauro, 2017). During the early stages of karstification, fractures caused by structural and depositional changes concentrate fluid flow in both lateral and horizontal directions in the subsurface (Klimchouk and Ford, 2000; Li et al., 2020; Meeder and Harlem, 2019; Sauro, 2014; Wray and Sauro, 2017). Aquifer hydraulic conductivity is further influenced by lithological changes in permeability, porosity, and mineral stratigraphy influencing how well fluids move through the aquifer (Anderson et al., 2009; Halihan et al., 1998; Magen et al., 2014; Wray, 2009). Therefore, the identification and quantification of parameters within inception horizons will serve as key data in identifying the controls of karst or pseudokarst development.

1.2 Soils Piping Controls

Unconsolidated or weakly consolidated sediments will be referred to here as soils. Similar to karst, soil weathering can create many karst-like features such as blind gullies, sinkholes, and gully windows (Bernatek-Jakiel et al., 2018). However, the process behind gully formation stems mainly from the mechanical removal of sediment along fluid flow lines and is called soil piping. Over time, soil pipes that begin as small conduits enlarge from the physical removal of mass along flow lines forming karst-like conduits. The internal erosion of soil pipes is dependent on how well the pipe is maintained (Bernatek-Jakiel and Poesen, 2018; Nadal-Romero et al., 2011; Wilson et al., 2013; Wilson et al., 2016; Wilson et al., 2018). Unlike aquifers that contain a cementing matrix, like

carbonates, soils cohesiveness originates in the amount soil structure and moisture content of the sediment. Variations in particle sizes and moisture affect the cohesive strength of the sediment potentially leading to collapse within soil pipes (Bernatek-Jakiel et al., 2020; Bernatek-Jakiel and Poesen, 2018). For example, under saturated conditions sediments dominated by sand sized particles collapse more readily than those dominated by clay grains. In fact, the stability of clay dominated sediments is so great that the internal erosion processes that cause collapse in sands do not occur in clays (Bernatek-Jakiel et al., 2020; Nadal-Romero et al., 2011). For a conduit to resist collapse and transport sediment the conduit must be dominated by silt sized particles, as they allow for the internal erosion of sediment while maintaining the cohesive strength of the conduit (Bernatek-Jakiel et al., 2020; Nadal-Romero et al., 2011). Ultimately, current knowledge on soil piping has attributed the development of the pipe to physical, lithological, and chemical characteristics of the soil sediment (Ali et al., 2011; Anderson et al., 2009; Bernatek-Jakiel et al., 2020; Bernatek-Jakiel and Poesen, 2018; Graham et al., 2010; Peng et al., 2016; Wilson et al., 2016; Wilson et al., 2018).

In soluble hard rock aquifers, the physical contribution to inception horizons comes from contrasting permeability located in secondary porosities like bedding planes and faults (Filipponi et al., 2009). However, as soils have yet to undergo cementation, structural deformations are not commonly propagated. Instead, the physical control on piping can often be generated by the permeability contrast at the soil-bedrock interface (Bernatek-Jakiel and Poesen, 2018; Bruthans et al., 2012; Gjettermann et al., 1997; Graham et al., 2010; Wilson et al., 2016). The soil-bedrock interface, similar to a bedding plane, constitutes permeability changes established by a physical and lithological change

in the sediment stratigraphy. Like permeability changes due to secondary porosity, lithological permeability changes cause flow lines to adjust to permeability differences within the soil structure moving fluids into previously un-infiltrated pathways (Graham et al., 2010; Peng et al., 2016).

Lithological changes in soils not only affect how sediment responds to chemically aggressive groundwater, but also the cohesive strength of the rock (Bernatek-Jakiel et al., 2020; Bernatek-Jakiel and Poesen, 2018). In karst, the lateral transport of groundwater through the aquifer may develop caves along an inception horizon due to the enlargement of pathways by dissolution of chemically cemented soluble rock. Distributions of grain size and mineral composition make particular areas of the soils more susceptible to dissolution or piping. Due to soils not being cemented, fluid moves through the soil along permeable pathways removing and transporting friable solids from along the pipe wall (Moore et al., 2010). A laboratory study conducted by Nadal-Romero et al (2011), demonstrated that the most susceptible piping horizon contained grain sizes of 8.8% clay, 79.8% silt, 11.4% sand, and was composed of 14.6% $CaCO_3$. The grain size distribution of less erodible beds was 20% clay, 74% silt, 6% sand, and a $CaCO_3$ composition of 0%. The author attributed the sediments resistance to piping to the stabilization by a higher clay content and the lower percentage of $CaCO_3$ particles in the observed samples. The combination of lithological characters determine how well the pipe enlarges due to dissolution and piping. While soil pipes with too little cohesion will collapse, pipes with too much cohesive soils will not erode (Bernatek-Jakiel et al., 2020; Moore et al., 2010; Wilson et al., 2018). Most soils contain varying grain size compositions, only few soils contain the necessary cohesive strength that permit the development of soil pipes

(Bernatek-Jakiel et al., 2020). Although soil piping may also result from dissolution, the dissolution process is slow and ends up just weakening the soil pipe walls (Bernatek-Jakiel et al., 2020; Dreybrodt, 1980). Once the soil pipes drain, dissolution stops and piping continues (Bernatek-Jakiel et al., 2020). Therefore, the enlargement of conduits within unconsolidated soils and the development of gully landforms are the result of rapid flow, greater internal erosion, and mass failure of pipe walls and roofs, which are all products of mechanical piping (Wilson et al., 2016; Wilson et al., 2018).

1.3 Pseudokarst

Sandstones are most commonly composed of a quartz grain matrix and cement which can range in composition. Other compositions exist, but many studies of pseudokarst focus on quartz arenite sandstones (Aubrecht, 2012; Mecchia et al., 1999; Mecchia et al., 2019; Piccini et al., 2009; Wray, 2009; Wray and Sauro, 2017). Due to the relatively low solubility of the quartz matrix, a focus on the dominant role of widening joints by chemical etching and subsequent detachment of quartz grains has been the primary focus of processes causing pseudokarst (Doerr, 1999). Martini (1979) defined arenization as dissolution of matrix along crystal boundaries causing an increase in the total rock porosity and making the rock less coherent and more susceptible to mechanical erosion. Arenization as a process includes both the chemical dissolution of soluble minerals and the mechanical piping of the less soluble materials. This process results in landscapes that are similar to both traditional karst and gullies, i.e. they contain sinkholes, caves, blind valleys, gully windows, among others (Bernatek-Jakiel and Poesen, 2018; Wilson et al., 2018). Similarly, pseudokarst result from differences in physical, lithological, and chemical components within the rock (inception horizons; (Filipponi et

al., 2009). Previous publications discuss that this interaction of different processes occurs to generate pseudokarst in quartz sandstones, however, how dissolution and piping work in tandem to create these landscapes has not yet been described (Mecchia et al., 2019; Sauro, 2014; Wray and Sauro, 2017). This thesis will quantify the hydraulic controls that contribute to pesudokarst formation within friable aquifers through the process of piping in a field setting.

1.4 Project Statement

Pseudokarst occurrence represents a spectrum that utilizes both dissolution and piping processes (**Error! Reference source not found.**). While the dissolution of soluble carbonate aquifers is heavily researched, pseudokarst development in insoluble friable rock has primarily focused on the dissolution of the sediment, neglecting the significance of the piping mechanism in pseudokarst formation (Mecchia et al., 2019; Sauro, 2014; Wray and Sauro, 2017). This study quantifies the mechanical hydrological controls required for pseudokarst formation in poorly consolidated lithologies. Based on observed data we hypothesize that differences in vertical permeability result in a rapid fluid response to generating piping erosion. During and after storm events the gradual water table recession causes a variation in magnitude and duration of both pseudokarst forming processes along flow paths allowing more time for dissolution of less soluble minerals. We tested this hypothesis in a field setting by identifying the dominant groundwater flow paths using land surveying, temporal electrical resistivity imaging (ERI), and quantifying the hydraulic gradient along the flow paths.

This study demonstrates that preferential flowpaths though fine grained portions of the lithologic section control the hydraulic parameters of the system and results in

arenization occurring along preferential pathways in a siltstone. Land surveying coupled with electrical resistivity imaging delineated the location of preferential pathways that facilitate the mechanical weathering of rock. The extent of groundwater infiltration into the aquifer surrounding the preferential pathways was identified using Temporal Electrical Resistivity Imaging (TERI). The TERI further defined how far chemically aggressive fluids may reach into the surrounding aquifer by identifying the areas of largest electrical conductivity changes along the preferential pathways. Hydraulic data was also collected to demonstrate that water table fluctuations above and below the pseudokarst structure are disproportional, and result from permeability differences along preferential flow paths. The infiltration of chemically aggressive fluid into preferential pathways, was then demonstrated by showing that groundwater EC decreases immediately after storms with a long period to return to baseflow conditions. Hydraulic gradients were calculated and compared to hydraulic gradients needed to induce the internal erosion of preferential flow paths.

Figure 1. 1 The Karst-Pseudokarst-Gully spectrum

CHAPTER II

2.0 SITE DESCRIPTION

A field research site in Stillwater, Oklahoma, U.S.A. was used to evaluate the hydrological controls on a pseudokarst formation in a field setting (Figure 2.1). Stillwater receives an average precipitation of 970 millimeters of rain per year, with the wet season being April to September. The climate classification is warm and temperate with an average temperature of 16°C. The topography of the site is a flat plateau with a steep slope with sinkholes and gullies ending a large pond called Lightning Lake (Figure 2.1). The Grainola-Lucien Complex soil is located above 291 meters above mean sea level, (amsl) and is a rocky, well-drained soil, that does not pond or flood during rain events. However, the Grainola-Ashport Soil below the 291 meters elevation grade to a silty clay loam and frequently pond with negligible runoff. The difference in soil composition correlates to the type of bedrock across the site (**Error! Reference source not found.**2.2).

The bedrock at the site is the Garber Wellington Formation (GWF) is a Permian sandstone interbedded with indistinguishable siltstones, mudstones, shales and sometimes dolostone to pebble conglomerates (Breit et al., 1990). While the geology is mapped as the Wellington formation only (Breit et al., 1990), the broader group is often referred to

based on interbedded sandstones and siltstones and will be referred to by the broader terminology. Compositions of minerals within the sandstones and mudstones of the formation have been quantified to be quartz (82%,34%), kaolinite (4%,4%), hematite (2%,7%), and illite (10%, 57%), respectively (Breit et al., 1990). The sandstone observed in the formation is a mix of quartz arenite to sub arenite, very fine – medium grained, well to poorly sorted sediment with an average porosity of 36%. Pores in the sandstone portions of the aquifer are commonly observed to contain coatings of authigenic minerals like illite that result from the dissolution of framework grains (Breit et al., 1990). The GWF is located just below the ground surface on the site outcropping at 296m AMSL throughout the site. The base of the GWF at the site is unknown; however, as the entire thickness of the formation ranges between 240-305 m. Sandstone in the GWF compromises over 75% of the total sediment (Breit et al., 1990). Interbedded shale can be 1.5-15m thick and contain high proportions of clays and silts, reducing permeability of the aquifer. However, sand and silt content of the shale beds increase in the upper part of the aquifer (Carr et al., 1977). The GWF is fine grained and poorly cemented, which reduces permeability, but is also the most productive aquifer in central Oklahoma (Carr and Marcher, 1977).

The study site contains numerous landforms that resemble features observed in karst environments such as, blind valleys, sinkholes, and discharging springs. This study will refer to the structures that resemble blind valleys as gullies, as they are the result of

both dissolution and soil piping weathering processes. This study focused on a gully at the northeast portion of the field site (**Error! Reference source not found.**.1). Sinkholes at the site are commonly less than 0.3 m in diameter and located along the topo or center of the topographically steep slope at the sandstone/siltstone contact (Figures 2.1 and 2.2). Some sinkholes lack enough cover that underlying bedrock is observable, and one sinkhole in particular created a 0.6 m large void space beneath the landowners' garage floor. Springs follow the trend of a fracture zone oriented oblique to a regional fault, which coincide with the regional stress field (Figure 2.2). The Garber Ridge Spring is an ephermal spring located at the top of the gully, and Trinity Point Spring is located within the lake and is a limnocrene seep that is expected to flow year round. Fluids have been observed discharging from the Garber Ridge Spring whereas only gas bubbles and lower electrical conductivity fluids were noted at Trinity Point Spring due to its location in the lake.

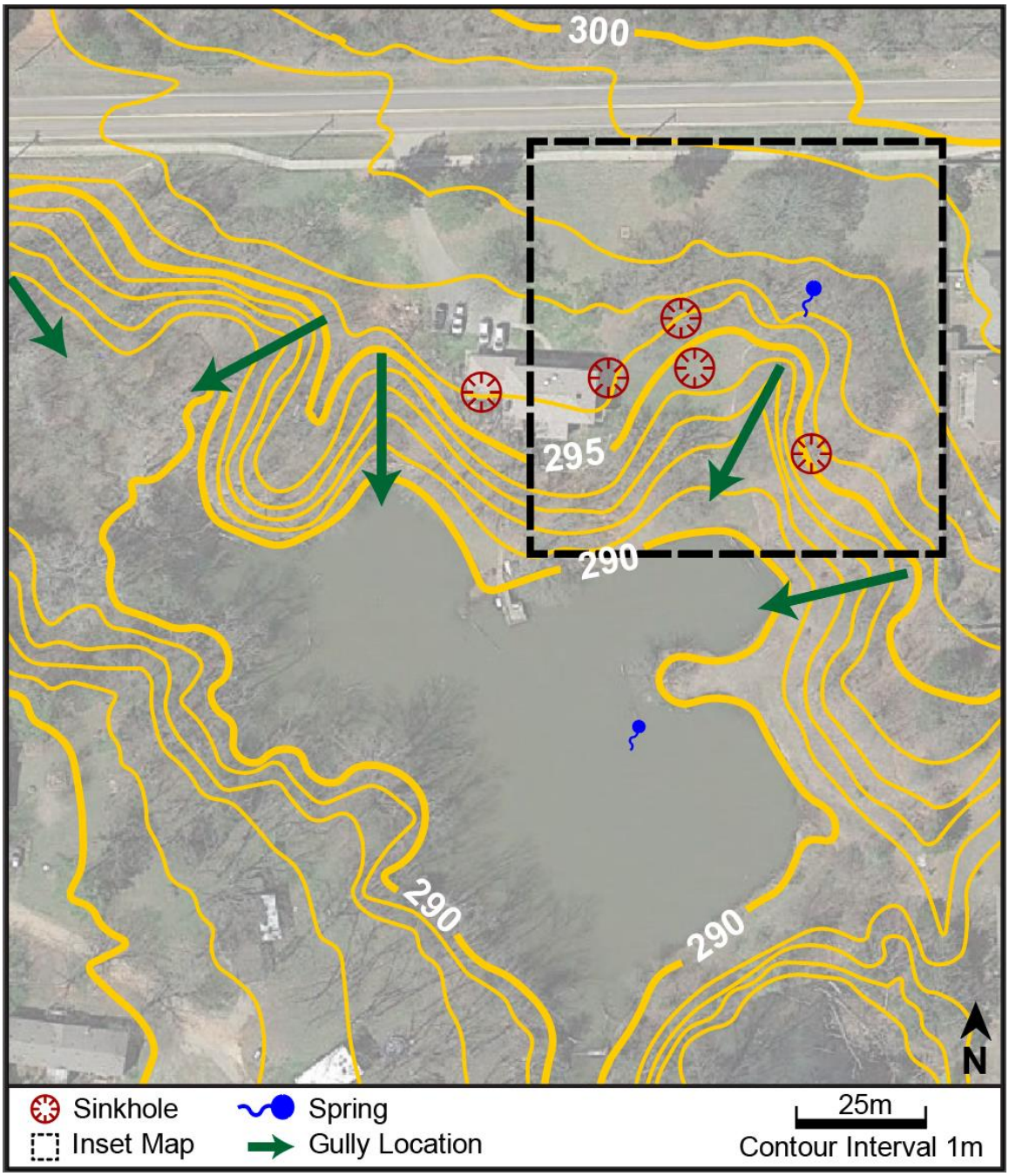

Figure 2.1 Topographic map of the Lightning Lake Research Site. Sinkhole locations follow the sandstone rock boundary closely (contour 296 meters). For detail see Figure 2.2. The inset map is the location of ERI lines used in the geophysical results section.

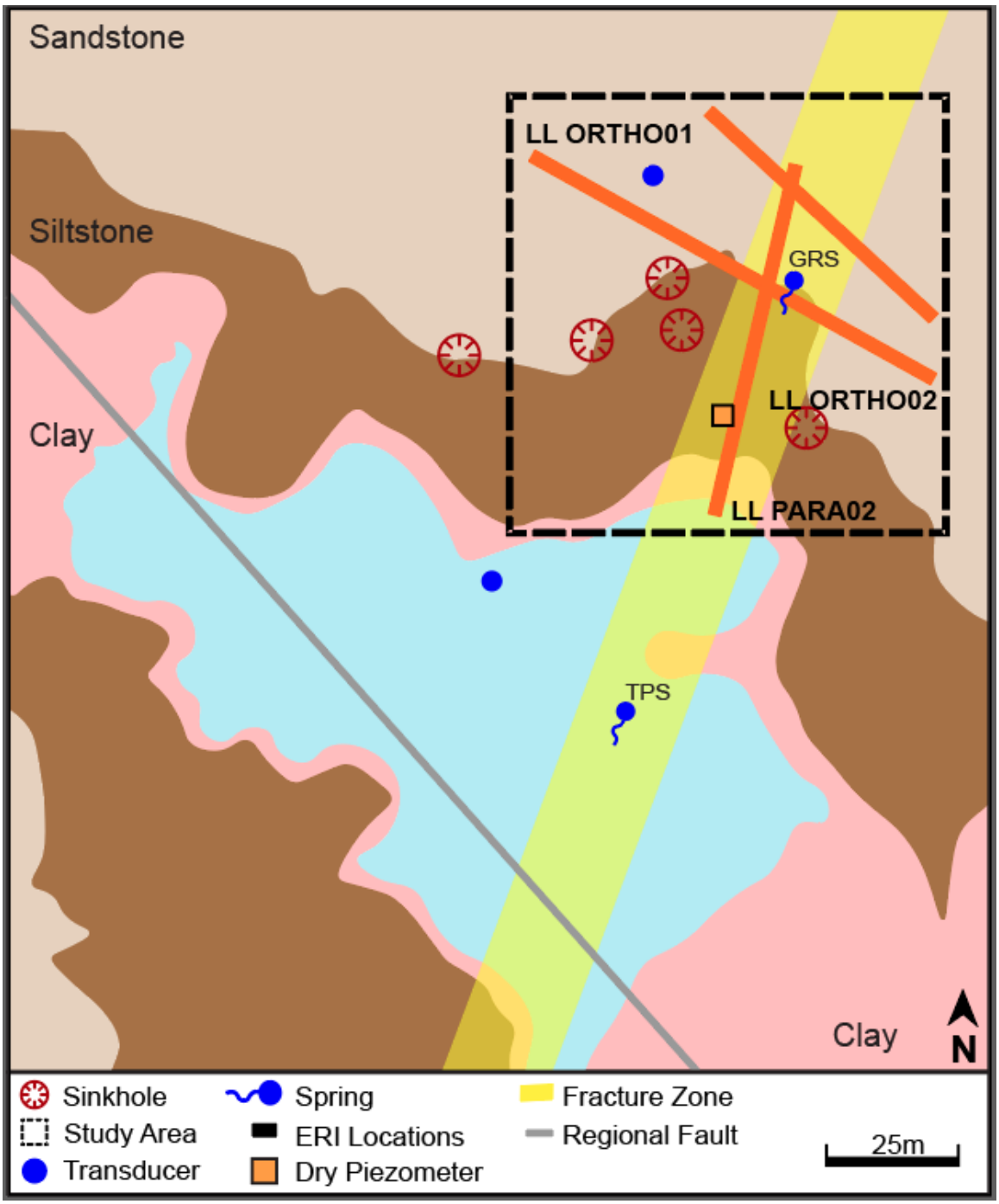

Figure 2. 1 Surface lithology map of the Lighting Lake Research Site. Sinkhole locations follow sandstone rock boundary closely (Contour 296 meters). The inset map is the location of ERI lines examined closely in the ERI results section. Garber Ridge Spring (GRS) and Trinity Point Spring (TPS) are indicated in the figure.

CHAPTER III

3.0 LITERATURE REVIEW

Pseudokarst regions consist of karst-like landforms produced by processes other than dissolution or corrosion (Ford and Williams, 2013). Pseudokarst structures occur in many different geologic settings and lead to the formation of similar landscapes throughout the world. Although these landscapes resemble similar structures, the processes that cause the aquifer's structure may be immensely different from one another. For example, magma that migrates through volcanic rock creates hollowed out lava tubes, or rheogeneic pseudokarst, while, melt waters moving beneath glaciers form structurally similar, tube-like glacier pseudokarst (Halliday, 2007). Confusion in what processes influence pseudokarst formation in different geologic settings can lead to a misunderstanding of processes controlling at risk aquifers. Therefore, it is pivotal to understand pseudokarst formation according to the geologic setting and processes controlling the pseudokarst development (Halliday, 2007).

Sandstone pseudokarst formation results from a combination of chemical and mechanical weathering processes that alter the characteristics of the sandstone aquifer. Composed of primarily sand sized quartz minerals, sandstone was presumed to be resistant to chemical weathering however, the chemical weathering of sandstone

pseudokarst takes place at soluble detrital grains and in authigenic cements within sandstone aquifers (Datta et al., 1996; Doerr, 1999). While detrital grains like feldspars, amphiboles, and micas, are quickly dissolved during diagenesis, authigenic cements can be precipitated from the ionic species left behind after dissolution (Datta and Tyagi, 1996). Cements such as, calcites, clays, and iron oxides lithify unconsolidated sandstones during diagenesis by filling in available pore spaces and eliminating the pathways of transport for chemically aggressive fluids (Datta and Tyagi, 1996). Although, these cements may precipitate under thermodynamically stable conditions they can also be dissolved just as easily (Datta and Tyagi, 1996). Both soluble detrital grains and authigenic cements represent the locus of chemical deformation within sandstone aquifers, therefore, understanding how diagenetic processes aid in the alteration of these components will help to delineate the controls of pseudokarst formation (Datta and Tyagi, 1996).

Diagenetic processes vary with depth. During shallow burial (eogenetic) diagenesis, thermodynamically aggressive meteoric fluids may come in contact with any soluble minerals within sandstones causing the redistribution of permeability and porosity within an aquifer (Klimchouk et al., 2000; Moore et al., 2010; Vacher et al., 2002). Martini (1982) noted that the formation of sandstone pseudokarst did not require the complete dissolution of sandstone rock, but only a 20% increase of porosity for karst-like structures to form. During the deep burial (telogenetic diagenesis) permeability is limited within the pore spaces of the aquifer due to the removal of interconnected pore spaces resulting from cementation and compaction. As the diagenetic stage changes from eogenetic to telogenetic the influence of meteoric water to dissolve or precipitate aquifer

material also changes (Hartkamp et al., 1993). During this intermediate (mesogenetic diagenetic) stage, thermodynamically unstable minerals like, hematite, aluminosilicate, carbonate, feldspar, and amorphous quartz can be dissolved from or precipitated into aquifer pore space according to the chemical affinity of the fluids in the subsurface (Dutta et al., 1986). The interaction between burial depth, meteoric water chemistry, and fluid circulation subsequently influence how fluids migrate throughout the subsurface. Shallowly buried eogenetic aquifers often undergo weakly to almost nonexistent cementation due to the circulation of the chemically aggressive fluids resulting in very friable rock (Worden et al., 2003). Lack of cementation in eogenetic aquifers causes friable rock to become more susceptible to mechanical piping then more cemented telogenetic aquifers.

In sandstone aquifers, a combination of both mechanical piping and chemical dissolution of rock leads to the formation of karst-like structures. Wray and Sauro (2017) defined the formation of karst-like structures resulting from the chemical dissolution of cements along crystal boundaries and the mechanical piping of friable low solubility rock matrix as arenization. Arenization, is not necessarily limited to sand grains, but can be observed in any aquifer with a combination of soluble cements and insoluble matrixes (Halliday, 2007). Although dissolution may not be the dominating process of pseudokarst formation, Jennings (1983) suggested that it was an essential precursor to mechanical piping of sediment grains. Therefore, the quantification of the aquifer characteristics resulting from diagenetic alteration can provide the parameters needed for understanding how fluids are transported through the aquifer.

3.1 The Balance Between Two Endmembers

The formation of sandstone pseudokarst represents a complex spectrum between chemical dissolution and mechanical piping. Current literature defines landscapes created by chemical dissolution of soluble species as karst landforms (Ford and Williams, 2013), while structures created as a result of mechanical piping are defined as gully landforms (Wilson et al., 2018). Differentiation between the two landscape processes has caused structures to be interpreted as the result of one endmember rather than a combination of both (Ford and Williams, 2013; Halliday, 2007; Wilson et al., 2016). Although both processes result in similar landforms, studies have yet to demonstrate the interrelationships between endmember dissolution and endmember piping in a sandstone pseudokarst field setting.

3.1.1 Chemical dissolution endmember

The chemical dissolution endmember results in characteristic karst landforms throughout the world (Ford and Williams, 2013). Karst landscapes originate from the chemical removal of soluble aquifer mass along preferential groundwater flowlines (Ford and Williams, 2013). Chemical dissolution of soluble rocks like carbonates and evaporates cause the enlargement of conduits and the formation of sinkholes, caves, and other karst structures (Ford and Williams, 2013). Subsequently, after the dissolution of soluble aquifer components, the piping of residual material continues the process of conduit enlargement (Ford and Williams, 2013). Although, both dissolution and piping participate in the formation of karst landscapes, the process is dominated by chemical dissolution (Ford and Williams, 2013). The karstification of a landscape requires the presence and development of preferential flow lines, which facilitate the transport of

under saturated fluids that are able to dissolve the rock body (Dreybrodt, 1980; Ford and Williams, 2013). Preferential flow paths direct the continual flux of aggressive under saturated groundwater to conduits, focusing dissolution along these paths (Filipponi et al., 2009; Meeder et al., 2019). Preferential pathways develop from the formation of inception horizons (Filipponi et al., 2009; Piccini and Mecchia, 2009; Sauro, 2014). Inception horizons represent the part of the rock succession that is particularly susceptible to the development of karst conduits due to physical, lithological, and/or chemical deviation from the predominant aquifer characteristics (Filipponi et al., 2009; Wray and Sauro, 2017). Each component of an inception horizon presents its own importance to the development of the preferential pathway and ultimately to the karstification of the aquifer. For example, the physical component of an inception horizon is represented by the spatial distribution and pattern of fractures or discontinuities (Wray and Sauro, 2017). The presence of faults, joints, bedding planes, and other discontinuities permit the vertical and horizontal transport of groundwater through the aquifer. The absence of these structural discontinuities restricts the infiltration of aggressive groundwater to the external regions of the aquifer, preventing the karstification of the rock (Klimchouk and Ford, 2000; Worthington et al., 2001). While discontinuities permit groundwater infiltration, lithological characteristics, such as permeability, direct ground water flow. Many times, preferential pathways develop as the result of a low permeability horizon preventing the downward percolation of groundwater (Graham et al., 2010; Marco and Pierre-Yves, 2008; Nieber et al., 2010). The lateral transport of fluids along low permeability horizons within the aquifer causes the enlargement of preferential pathways, increasing the conduits capacity to transport groundwater (Aley et al., 2012; Filipponi et

al., 2009). Conduits located in the vadose to epiphreatic zone often receive rapid influxes of fresh groundwater during rain events (Halihan et al., 1998a; Halihan et al., 1998b; Mecchia and Piccini, 1999; Nieber and Sidle, 2010). Variations in conduit diameter along the flow path causes the buildup of hydraulic pressure within the conduit (Halihan et al., 1998b). This results in the reversal of fluid flux from the conduit into the surrounding aquifer. Pore spaces of the surrounding aquifer are then flushed with fresh fluids from the conduit over a limited distance from the conduit. The thermodynamic stability of the surrounding aquifer govern the time required for dissolution and the rate of karst development (Dreybrodt, 1990a).

While aquifers containing stable mineral constituents may resist chemical weathering for eons, aquifers composed of evaporate material can develop karst landscapes within days (Ford and Williams, 2013). The chemistry of the lithologic layering determines the response of the inception horizon to aggressive fluid infiltration. As lithologic chemistry can vary from aquifer to aquifer, so does the type of fluid needed to dissolve the rock. Meteoric waters provide under saturated fluids to the water rock interface, while the disassociation of water produces H^+ and OH^- ions. At the mineral-fluid interface, the carbonate portion of calcite, CO_3^- becomes hydrated with H^+ and undergoes acid dissolution. Causing the $CaCO_3$ calcite to disassociate, releasing Ca^{2+} and HCO_3^- into the groundwater (Ford and Williams, 2013). The speciation of carbonate minerals can be delineated by assessing the geochemical components of the groundwater (Hem, 1985). For this, stoichiometric ratios of the groundwater are typically used to statistically prove that the hypothesized chemical reaction is occurring (Hem, 1985). These are called index ratios. In sandstones, index ratios are integral in determining

chemical reactions undergoing other dissolvable minerals like iron oxides, feldspars, and clays (Price et al., 2003).

Due to the multitude of mineral compositions contained in sandstones, a major ion chemical analysis must be done to quantitatively assess index ratios. Common sandstone speciation that can be readily observed in fluid chemistry include the alteration of minerals like feldspars and calcites. **Error! Reference source not found.** displays the chemical equations for chemical alteration and dissolution reactions of feldspars and calcites respectively (Hem, 1985). A comparison of the concentrations of aqueous products solution to index ratios present within the equation will identify if the observed reaction is of primary importance at the site. However, difficulty arises when attempting to understand the speciation of minerals that are in high abundance or constantly exchanging with the groundwater (Price and Velbel, 2003). The occurrence of iron oxides and clays in sandstones demonstrate this difficulty as their chemical reaction signature can lead to the formation of multiple minerals and clays, making information acquired for a single index ratio quite ambiguous (Price and Velbel, 2003). Therefore, the use of mineral stability diagrams to delineate the stability of a mineral at a particular pH-Eh environment is required to correctly asses the geochemical environment(Hem, 1985). Many studies have used the index ratio in tandem with mineral stability diagrams to verify their assumptions of what chemical process are taking place (Gibbs, 1970; Hem, 1985; Katz et al., 1998; Price and Velbel, 2003; Viollier et al., 2000). Physical, lithological, and chemical characteristics of the aquifer play a vital role in the dissolution and enlargement of conduits and influence karstification accordingly(Filipponi et al.,

2009). Therefore, analysis of each individually is necessary for understanding what processes aid in the formation of pseudokarst.

Dissolved Mineral	**Equation**	**Ions in Solution**
Calcite	$CaCO_3 + H_2CO_3 \leftrightarrow Ca^{2+} + 2HCO_3^-$	Ca^{2+}, HCO_3^-, H^-
Potassium Feldspar	$2KAlSi_3O_8 + 2H^+ + H_2O \rightarrow Al_2Si_2O_5(OH)_4 + 2K^+ + 4SiO_2$	K^+
Plagioclase Feldspar	$CaAlSi_3O_8 + 2H^+ + H_2O \rightarrow Al_2Si_2O_5(OH)_4 + Ca^{2+}$	Ca^{2+}

Table 1 Dissolution equations and products in aqueous form in groundwater.

3.1.2 Soil piping endmember

The soil piping endmember is composed of similar inception horizons that lead to the removal of solid material from the aquifer along permeable pathways. Due to the unconsolidated nature of soil sediments, mechanical erosion dominates the soil piping process. Soil piping leads to the formation of gully landscapes in unconsolidated soils (Wilson et al., 2018). The lack of consolidation within soils results in the collapse of soil pipes before meter scale diameters can be reached (Anderson et al., 2009; Wilson et al., 2016; Wilson et al., 2018). This has resulted in studies focusing on either physical and lithological or chemical aspects of the inception horizon in soils rather than how these parameters influence the conduits hydrological response to groundwater flow (Bernatek-Jakiel et al., 2020; Bernatek-Jakiel and Poesen, 2018; Wilson et al., 2016). Wilson et al. (2016) defined permeability contrasts, hydraulic gradients and collapsible medias as the characteristics of the aquifer that made it more susceptible to gully formation, while Bernatek-Jakiel et al. (2020) identified that it was the content of major oxides, soil particle size, biologic activity, and porosity that influenced gully formation. Similar to karst formation, gully formations result from the enlargement of conduits along physical, lithological, and/or chemical differences in the aquifer flow path (Filipponi et al., 2009). However, the term inception horizon has only been applied to karst formations, even though similar controls have been observed in soils.

In soils permeability contrasts induced by lithological differences in the soil strata promote the lateral migration of groundwater fluids (Wilson et al., 2018). Similar to karst aquifers, fluids are percolated downward until they reach a low permeability boundary. At the boundary fluid can be transported laterally through a flow pipe capable of

transporting solid particles. During storm events, the rapid infiltration and propagation of the storm pulse through the soil pipe leads to the entrainment of soil grains within the soil pipe conduit (Anderson et al., 2009). As the hydraulic pulse moves through the aquifer, flow velocity is increased (Anderson et al., 2009; Wilson et al., 2016). Variations in conduit diameter and hydrologic flux along the flow path magnify the flow velocity changes within the conduit (Graham et al., 2010; Wilson et al., 2016; Wilson et al., 2018). The continual migration of storm pulses along flow paths therefore results in the erosion and enlargement of the conduit, ultimately leading to the formation of collapse structures like gullies (Wilson et al., 2018). Therefore, understanding how the aquifer attenuates hydraulic fluxes along preferential pathways is integral to determine the time required for landscape formation.

Velocities within conduits and soil pipes can be highly variable, depending on the hydraulic flux applied to the pathway (Graham et al., 2010; Wilson et al., 2018). Therefore, different rain events can result in variable sizes and amounts, of sediments being transported through the pipe. Grains contained and transported along permeable pathways can be a combination of allogenic and autogenic sediments, providing a source of highly variable grain sizes dependent on the physical and chemical origin of the sediments (Herman et al., 2012). In soils, the silt sized particles provide the structural cohesiveness that is normally lacked by unconsolidated sediments. Therefore, soils pipes are often observed in aquifers containing fine – medium grained sized particles, in particular silt sized (Bernatek-Jakiel et al., 2020; Bernatek-Jakiel and Poesen, 2018; Nadal-Romero et al., 2011). This being said, subcutaneous sediment transport is similar to open channel fluid flow where sediments can be either a part of bed load or suspended

load that is transported through the pipe (Herman et al., 2012). Since the velocities and grain sizes being transported during the suspended and bedload migration of sediments will be discussed in the next section we will provide a very simplistic overview of the loads here. Suspended load is the portion of sediment transport that always remains in suspension (Herman et al., 2012). Bedload sediment transport is the sediment that may be entrained in flow during high hydraulic fluxes and tends to drop out of suspension soon after the flux has dissipated (Herman et al., 2012). Grain sizes and velocities required to entrain both suspended load and bedload sediments is highly dependent on the available grains and hydraulic fluxes applied (Herman et al., 2012). For example, the velocity required to transport the gravel sized particles in a karst aquifer may be much higher than that required to transport a clay sized particle in a soil pipe. As particle transport is not the dominating weathering process in karst, most studies neglect to assess the influence flow velocity has on karst formation (Ford and Williams, 2013). However, sediment transport velocity in soil has been quantified in numerous studies as well as the amount of sediment removed along a particular pipe (Anderson et al., 2009; Nadal-Romero et al., 2011; Wilson et al., 2016). A pipe flow velocity of around 0.0005 – 0.66 m/s is required to transport the fine silt to sand fine sized particles along a soil pipe.

3.2 Sandstone/Siltstone Pseudokarst

The intermediate process of arenization involves both dissolution and piping mechanisms to create pseudokarst landforms in rocks composed of largely insoluble particles and soluble cements. The degree of pseudokarst development is ultimately related to the arenization processes occurring at pore and formation scales within the aquifer (Wray and Sauro, 2017).The variability of aquifer characteristics such as, the

degree of cementation, the percentage of soluble-insoluble constituents, and grain size distribution within the aquifer determine how the aquifer responses to arenization (Wray and Sauro, 2017). Although many size particles may be present in the rock matrix, for arenization to occur the majority of sediments must be sand or silt sized particles. Generally, the process is called sandstone pseudokarst and that convention will be used here although the possibility of other grain sizes is acknowledged (Wray and Sauro, 2017).

Much like the karstification and soil piping endmembers, the presence of an inception horizon and the development of a preferential pathway are fundamental for arenization processes (Mecchia and Piccini, 1999; Mecchia et al., 2019; Wilson et al., 2018). The development of pseudokarst landscapes due to arenization occurs at both pore and formation scales. Characteristics of the unsaturated and epiphreatic zones (the intermittently flooded zone) play a large role in the responses of the chemical and hydrological aspects of the preferential flow path(Wray, 2009). At the pore scale influxes of fresh oxic and somewhat acidic fluids cause the local dissolution of soluble mineral components (Onac et al., 2011). If sufficient enough organic material is supplied to the epiphreatic zone the redox potential (Eh) can be potentially altered, moving from highly oxic to slightly reductive (Onac and Forti, 2011). If the residence time of fluids is long enough the organic material and available oxygen may be used up, changing the redox potential from oxic to slightly reducing ranging from an +0.4 to +0.6 within this epiphreatic zone (Onac and Forti, 2011). As many diagenetic components result from equilibrium reactions, cements and minerals stable under one redox conditions will not be stable under another (Walker et al., 1978). At the formational scale, conduit diameters are

governed by the erosion and piping of material within them (Wilson et al., 2018).The internal piping of sediment is highly dependent on the sizes of bedload and suspended load grains as well as the hydraulic flux being applied to the preferential pathway. Therefore, an approach of identifying pore scale dissolution processes and formation scale piping processes is needed to delineate the controls on pseudokarst formation.

3.2.1 Pore Scale Processes

During diagenesis, pore spaces within sandstones become filled with cements reducing the permeability of the aquifer (Walker et al., 1978). Pore filling material removed during the arenization process constitutes both aspects of dissolution and piping at the microscale. The dissolution of soluble cements increases void spaces between grains, weakening the cohesive strength of the aquifer (Wray and Sauro, 2017).Porosity enlargement permits the increase of permeability within interconnected void spaces, providing larger microscale pathways for fluid flow. As the voids develop into a preferential pathway, migrating groundwater fluids begin to pipe loosened grains away from their original location (Bernatek-Jakiel and Poesen, 2018; Wilson et al., 2018; Wray and Sauro, 2017). Both dissolution and piping processes work in tandem to enlarge void spaces through the removal of cements and grains together. Arenization of the microscale leads to the formation of macroscale preferential pathways, ultimately helping to form formation scale conduits (Piccini and Mecchia, 2009; Sauro, 2014; Wray and Sauro, 2017). The lithological component of the inception horizon plays a large role in controlling the rate of arenization (Mecchia et al., 2019). Above the preferential pathway, the vertical percolation of meteoric waters results in the dissolution of soluble components along the fluids pathway. During percolation through the vadose zone

residual meteoric water is held tightly to the grain surfaces due to adsorption at the fluids-grain interface (Dreybrodt, 1990a). The reaction time required to dissolve the grain is dependent on the solubility constant at the location of the reaction. Most of these minerals are never in equilibrium with the interstitial fluids (Walker et al., 1978). Therefore, the time required for dissolution is dependent on the saturation of the fluid at the water-grain interface (Walker et al., 1978). Over time, the dissolution of the cements begins to saturate the fluid at the interface, reducing the rate of dissolution at this location. To continue dissolution, fresh chemically aggressive water must flush out the saturated fluid (Vesper et al., 2004; Wray and Sauro, 2017). Along the preferential pathway, the lateral movement of groundwater results in the dissolution of the cements in the horizontal direction. Again dissolution rate is determined by the amount of thermodynamically aggressive water in contact with the soluble minerals. Rain events provide the aquifer with the necessary solvent to permit dissolution. However, during the storm events the velocity of the infiltrating fluids reduces the time for fluid-grain interaction (Katz et al., 1998; Vesper and White, 2004). Fluids at the water-grain interface have little time to complete their dissolution reaction and a reduction of the rate of dissolution occurs until the flow velocity slows (Dreybrodt, 1990a). During rain events, the microscale inception horizon becomes a flow tube for fresh water transportation, piping material as groundwater moves tortuously through the pore spaces of the aquifer (Nieber and Sidle, 2010). At these times, mechanical piping dominates the arenization process (Wilson et al., 2016; Wilson et al., 2018). Once the hydraulic pulse subsides, the freshwater at the fluid-rock interface continues to dissolve soluble grains, moving the fluid towards equilibrium. The dissolution and piping processes of

arenization at the microscale are important in that they develop the initial flow conduits that ultimately form the formational scale conduits observed in pseudokarst rock.

The dissolution of framework grains and the precipitation and dissolution of authigenic cements cause the alteration of fluid chemistry within interstitial pores of the aquifer (Walker et al., 1978). The chemical analysis of these interstitial fluids at periods of differential flow can provide temporal information on the exchange of ions at the fluid rock interface (Katz et al., 1998). Major ion analysis of fluid chemistry during high and low flow periods provide data that can help identify when dissolution occurs in the aquifer. Demonstrating this, Katz et al. (1998) monitored geochemical changes in the Floridian limestone aquifer collected groundwater samples at various times. Data collected, observed the changes in the concentrations of major ions, HCO_3, dissolved oxygen, and Calcium, delineating the occurrence of limestone dissolution (Katz et al., 1998). During times of high fluid flow, sampled fluids decreased in HCO_3^- and dissolved oxygen, while Ca decreased substantially, relative to periods of low flow (Katz et al., 1998). Times of low flow resulted in groundwater saturation with respect to calcite decreased throughout the entire study site (Katz et al., 1998). This is indicative of fresh under saturated water infiltration. In fact, during high flow periods, Na and Cl concentrations increased substantially. The study identified this flux of cations Na and Cl to originate from the infiltration of evaporated and then precipitated seawater. Another study analyzed groundwater migrating at the surface and within deep caves formed in arenite sandstone (-350m depth) (Mecchia and Piccini, 1999). Collecting concentration data for dissolved silica and SiO_2, they demonstrated that both fluids were under saturated above and below the surface (Mecchia and Piccini, 1999). However, during

high discharge events the silica load rose while the concentration decreased. Mecchia and Piccini (1999) concluded that although the load of silica rose during discharge events, the main source of dissolved silica originated from the rinsing of silica from underground dissolution sites (Mecchia and Piccini, 1999). Fluid chemistry analysis is a much needed verification tool and when used in tandem with petrographic analysis, can delineate the parts of the aquifer most susceptible to dissolution.

In sandstone, the dissolution of grains and cements result in macro and micro alterations of the aquifer structure (Shanmugam et al., 1988; Walker et al., 1978). The complete or partial dissolution of grains can result in the development of void spaces. For the identification of grain dissolution, void space preservation is essential (Shanmugam and Higgins, 1988; Walker et al., 1978). Before dissolution, the migration of clays or precipitation of authigenic cements may cover the initial undissolved grain. After the grain is dissolved, the remaining sediment surrounding the grain may be all that demonstrates the presence of the initial grain (Walker et al., 1978). When the surrounding sediments collapse due to compaction stresses diagenetic history of the aquifer can be completely removed (Walker et al., 1978). Available void spaces can also be infilled with authigenic cements that can remove any existence of the previous void spaces formed from dissolution (Walker et al., 1978). Grain filling cements and intra grain voids represent precipitation and dissolution of cements respectively (Burley et al., 1986). The alteration of grains and cements controls how fluids migrate through the subsurface (Burley and Kantorowicz, 1986; Shanmugam and Higgins, 1988; Walker et al., 1978). Therefore, a thorough investigation of the aquifers petrographic structure is important to delineate dissolution processes controlling pseudokarst formation.

3.2.2 Formation Scale

The continual arenization of the interconnected pore spaces develops into the conduits that result in pseudokarst formation. Conduits within sandstones range in magnitudes from millimeter- to meter-scale (Wray and Sauro, 2017). Permeable pathways within these conduits enlarge their diameter permitting the transport of larger volumes of groundwater through the aquifer (Bruthans et al., 2012). During storm events, aggressive water moves through preferential pathways and infiltration flux increases through the conduit with hydraulic pressure increasing quickly (Halihan et al., 1998b; Katz et al., 1998). The increase in total hydraulic head increases flow velocity within the conduit and the fluid begins to entrain rock material of larger grain size. As the hydraulic pressure increases fluid flow is transported from the conduit to the surrounding aquifer (Moore et al., 2010). As discussed in the previous section, the aquifer surrounding the conduit is infiltrated with aggressive meteoric fluids permitting dissolution to occur in these locations and generating a halo of friable material (Moore et al., 2010). The diameter of this halo is dependent on the hydraulic pressure applied to the conduit, as this determines the depth of the aggressive fluids into the surrounding matrix (Moore et al., 2010). This is the location of dissolution at the formational scale. Once the storm pulse subsides the hydraulic pressure returns to transporting fluids from the surrounding aquifer to the conduit. Some portions of the aquifer retains a degree of fresh water for dissolution of cements and grains (Velde, 1995). The flushing of saturated pore spaces as a result of rapid infiltration at or near the water table results in the periodic infiltration of unsaturated meteoric groundwater (Katz et al., 1998). The influx of groundwater during storm events enlarges the conduit diameter by piping away the friable material

originating in the conduit walls. Piping also increases the depth of infiltration into the aquifer surrounding the conduit (Bruthans et al., 2012; Moore et al., 2010). Both microscale (pore) and macroscale (formation) infiltration, dissolution, and piping play major roles in the formation of pseudokarst landscapes.

The evolution of conduits by the fluidization and piping of sediment out of a sandstone aquifer was observed in the lab and in the field by Bruthans et al. (2012). Fluidization is the mobilization of sediments due to the local saturation of the aquifer, resulting in the reduction of tensile stress and subsequent mass wasting of the conduit (Bruthans et al., 2012). In the shallow phreatic zone, mass wasting from fluidization, causes the upward propagation of the vertical conduit. According to the data, a hydraulic gradient of between 0.005 - 0.02 was needed to facilitate a buildup of fluid large enough to establish a conduit velocity of 0.34 – 0.4 m/s (Anderson et al., 2009; Bruthans et al., 2012; Wilson et al., 2016). At this velocity, disaggregated aquifer material could be removed from the conduit (Ford and Williams, 2013). While in the vadose zone the hydraulic gradient required for fluidization is approximately 0.7 m/s. A similar evolution of conduits was modeled in a karst aquifer (Clemens et al., 1999). Modeling of phreatic fluid flow along an epikarst boundary produced three different phases of conduit development a) the initiating phase where conduits are enlarged by fourth ordered kinetics, b) the enlargement phase where the conduit is enlarged by first order kinetics, and c) the stagnant phase when enlargement rates and conduit flow velocity decrease (Clemens et al., 1999; Dreybrodt, 1990a). At the first phase, conduit velocity is around 10^-2 m/s and conduit diameter 5 – 10mm. Phase two increases the velocity to a magnitude of almost 1 m/s and a conduit diameter of 3m. At phase three, conduit velocity

and diameter rates begin to decrease to as the conduit becomes too large to support high velocities that contribute to first order kinetic reactions. In the last phase conduit walls become covered with clays hardening the inside of the conduit and preventing additional dissolution and erosion (Bruthans et al., 2012; Clemens et al., 1999). Phase three occurs when velocity decreases back to 10^-2 m/s and conduit diameter becomes >3m (Clemens et al., 1999).

Upon comparison of data from the enlargement of conduits in sandstone and karst aquifers values for conduit velocity are very much similar. Differences arise as sandstone conduits evolve from the head ward enlargement of fractures, while karst from the opposite. Also, the components of physical and chemical weathering respectively create unique responses along the conduit's pathway in both lithologies. However, as both structures result in the enlargement of conduit diameters pseudokarst formation in sandstones may be controlled by an individual process or both combined (arenization).

3.3 Formation Controls

Arenization results in the enlargement of conduits and the formation of pseudokarst structures along the direction of preferential flow paths. Hydraulic pulses from rain events, provide influxes of hydrologic energy into the conduit, permitting both mechanical and chemical weathering (Ford and Williams, 2013). Once in the aquifer, the hydraulic pulse causes oscillations in fluid flows along the flow path. Hydraulic parameters like hydraulic gradient, chemical aggressiveness of the fluid, groundwater residence time, recharge distance, and velocity quantify how energy is attenuated along lithological, chemical, and structural differences of the flow path (Mecchia et al., 2019).

A detailed observation of these parameters provides data sufficient enough to delineate the controls of arenization in a sandstone system.

Soil, carbonate or sandstone aquifers respond to hydrological energies differently, however they all create similar landscapes (Ford and Williams, 2013; Wray and Sauro, 2017). For each aquifer, the type of fluids required to form karst and karst like landscapes differs based on the chemistry needed to dissolve the aquifer (Ford and Williams, 2013). As karst landforms result from the chemical alteration (dissolution) of sediments, gullies form from the physical piping of soil material along a conduit pipe. Although the dominant weathering processes in carbonates and soils are respectively, dissolution and piping, both aquifers retain some portion of each weathering process (Bernatek-Jakiel et al., 2020; Ford and Williams, 2013; Halliday, 2007). However, current understandings of dissolved blind valley and piped gully formations are represented by an either/or conceptual model, where landforms originate from only one endmember of the dissolution-piping spectrum (**Error! Reference source not found.**) (Ford and Williams, 2013; Wilson et al., 2018). Studies of sandstone pseudokarst have also resulted in a similar one-sided quantification of the spectrum. This perspective is generally oversimplifying the occurrence of pseudokarst which is a natural middle ground for the dissolution-piping spectrum.

The current literature on sandstone pseudokarst landscapes focus on its formation in quartz arenite (Sauro, 2014; Wray and Sauro, 2017). The pseudokarst formation in quartz arenite has resulted mainly from the process of arenization (Wray and Sauro, 2017). This focus presents a bias in the understanding of how different compositions of sandstones influence the dominant weathering process within arenization. As quartz

arenite is a particularly pure sandstone (quartz >90%), dissolution of the matrix is a controlling factor in pseudokarst formation (Wray and Sauro, 2017). On the other hand, weakly bonded sandstones may not offer fluids sufficient residence times to dissolve aquifer materials, reducing the dominance of the dissolution process (Wray and Sauro, 2017). Consequently, the analysis of sandstones of a particular composition has limited the understanding of pseudokarst occurrence to only that based on well cemented sandstone aquifers.

Sandstones throughout the world represent unique combinations of physical, lithological, and chemical constituents that respond to weathering differently. The quantification of the controls on pseudokarst formation in sandstones of varying compositions will allow for an improved delineation of the controls on pseudokarst formation (Wray and Sauro, 2017). Therefore, to understand the uniqueness of pseudokarst formation within texturally variable sandstones, the parameters that lead to the formation of karst and karst-like landforms in consolidated karst and unconsolidated soils must be examined. The arenization of friable sandstone aquifers permit the opportunity to quantify both dissolution and piping controls on pseudokarst formations. As both processes occur simultaneously, we will comparatively analyze the factors that promote dissolution and piping processes in their individual environments. The information reviewed represents controlling variables that will be compared to the data we collect. We expect that reviewing hydrological, lithological, and formational controls on the arenization process will help to delineate the dominant controls of arenization on friable sandstone aquifers.

3.3.1 Hydraulic gradient

Most conduits in karst systems tend to develop where hydraulic gradients run parallel to structural discontinuities (Filipponi et al., 2009). The fluctuation of the gradient along these discontinuities can lead to the deviation of flow tubes in horizontal and vertical directions (Filipponi et al., 2009). During storm events, variable influxes of hydraulic pressures can cause the amount of kinetic energy to fluctuate, increasing or decreasing the total head in a particular area. Upon a rise in the water table, flow paths may reorganize, connecting pore spaces that were initially disconnected and dry to an effective flow network (Nieber and Sidle, 2010). Eventually fluids percolate to an inception horizon where they are transported laterally across a preferential pathway (Filipponi et al., 2009; Nieber and Sidle, 2010). At times of intense hydraulic flux, the increase in the aquifers hydraulic gradient causes the convergence of all fluid flow into the preferential lateral flow pipe (Halihan and Wicks, 1998a; Halihan et al., 1998b; Nieber and Sidle, 2010). The flux increase into the flow pipe causes the buildup of total head in the conduit as well as throughout the aquifer. In karst, this results in the rise of the water table and the increase of flow velocity and hydraulic pressure within the conduit (Halihan et al., 1998b). When the hydraulic pressure of the conduit exceeds the pressures in the surrounding aquifer, the hydraulic gradient reverses and fluid begins to flow from the conduit to into the surrounding sediments (Moore et al., 2010). Similar, occurrences have been observed in soils of a hillslope where groundwater fluids were stained with blue dye in an effort to identify water levels through flow pipes (Anderson et al., 2009). Upon the excavation of potential flow pipes, it was observed that in some locations, dye coated the entirety of a pipe diameter. The study concluded that the stained

fluid was restricted to the soil pipe unless a constriction in the pipe caused the increase in hydraulic head and the reversal of the gradient into the surrounding aquifer. In both karst aquifers and unconsolidated soils, the build-up of total head changes hydraulic gradients and can redirect or intensify the direction of flow (Halihan et al., 1998b; Moore et al., 2010; Nieber and Sidle, 2010).

The conduit diameter along flow pipes, may be highly variable depending on the flow paths response to inception horizons, resulting in the alteration of flow path characteristics (Ford and Williams, 2013). In karst, the incongruent dissolution of carbonate aquifers can cause the conduit diameter to enlarge from 0.01m to a diameter of several meters in a short amount of time (White, 2002). Highly variable conduit diameters may then be in close proximity to one another, transporting fluids from a relatively large to small conduit diameter. Transport through constrictions observed in karst aquifers, result in the increase of flow velocity and total head within the conduit (Halihan et al., 1998b). Soils on the other hand cannot maintain conduits with diameters >1m due to their unconsolidated structure (Wilson et al., 2016). Unlike soils, the karstic aquifer matrix is chemically cemented allowing for the development of large diameter conduits without collapse. In soils, the cohesiveness is dependent on the attraction between the individual grains (Wilson et al., 2018). For this reason, diameters of soil pipes rarely get over 0.5m. Total head in soils ranges around 10 – 60 cm during storm events, while values for total head in constricted karst conduits and 20 – 70 cm causing a rise of as much as 100 m of water table change in karst (Halihan et al., 1998b; White et al., 1995). In eogenetic (high porosity) aquifers, the above total head values can result in the reverse of hydraulic gradient from the conduit into the surrounding matrix, thus

causing the dissolution of matrixes holding the grains together (Moore et al., 2010). In similar weakly bonded aquifers, the increase in total head intensifies the hydraulic gradient and can lead to the amplification flow discharge and velocity. Both, fluid reversal into the matrix and amplification of flow velocity, lead to the removal of sediment grains from the conduit wall of eogenetic aquifers (Moore et al., 2010; Wilson et al., 2016). These fluctuations in the hydraulic gradient induced by changes in total head values within eogenetic aquifers may cause dissolution and piping processes to coexist at different rates along the flow path. Therefore, it is important to quantitatively define the hydraulic gradient within the pseudokarst formation.

3.3.2 Chemical Aggressiveness

The amount of dissolution observed during the process of arenization, is a function of the infiltration rate of chemically aggressive pore filling fluids. Although dissolution rates of soluble minerals may vary with climate, the dominant controlling factor when it comes to arenization of an aquifer remains to be the amount of chemically under saturated fluid interacting with the mineral surface (Wray and Sauro, 2017). While dissolution within sandstones has focused on quartz arenite aquifers, other types of sandstones can also be dissolved in part, if not entirely. Conduit evolution contributes to the dissolution rate of minerals within the aquifer. In fact, aggressive water circulation is controlled by the size of the conduit fluids are transported through (Clemens et al., 1999; Dreybrodt, 1990b). In the early stages of karstification of a carbonate aquifer, fluid circulation is limited due to the aperture width of preferential flowpaths (10^{-2} – 10^{-3} cm) (Dreybrodt, 1990a). The karstification of a rectangular fracture (initially at a width of 10^{-2} cm) within a 100 m block of carbonate rock was modeled by Dreybrodt (1980). It was

demonstrated that from 0-54,000 years' the dissolution rate remained at a slow fourth order rate only enlarging the fracture width and length, 1 – 10 cm and 4 m respectively. However, after 54,000 years a first order dissolution rate began to occur altering the width and length of the fracture to 10^2 and 100 m respectively in a matter of 10,000 years (Dreybrodt, 1990b). This change in rate of dissolution was attributed to drastic change in flow rate within the fracture. During the slow fourth ordered reaction period, the flow rate into the fracture was between 1 - 5 cm^3/s. Once at 54 000 years the flow rate increases drastically from 10 – 10^8 cm^3/s in less than 10,000 years. The influx of fresh aggressive fluids, or flushing rate, is directly proportional to the rate of dissolution within the aquifer. Flushing rate provides the aquifer with the fresh fluids necessary to dissolve soluble species. Another, important factor that controls the time available for aggressive fluid interaction with the aquifer is the fluid's residence time. Chemical aggressiveness of fluids is indirectly related to its residence time in the aquifer (Dreybrodt, 1990a). Fluid aggressiveness and residence times go hand in hand when evaluating controls on dissolution processes of soluble aquifers, (Dreybrodt, 1980; Ford and Williams, 2013; Wray and Sauro, 2017).

3.3.3 Fluid residence time

Aggressive fluid residence time in the aquifer controls the alteration rate of soluble minerals at the fluid – rock interface (Ford and Williams, 2013; Wray and Sauro, 2017). This interface is sometimes called a microsystem and it occurs where ever fluids are directly in contact with a soluble mineral species surface (Meunier et al., 2007). The rate of alteration (dissolution or precipitation) of a mineral species is highly dependent on the chemical potential differences within a flow path (Meunier et al., 2007). Fluids

migrating through preferential pathways of the aquifer often contain variable chemical potentials, that result in differential alteration where conditions are favorable (Meunier et al., 2007). Alteration of soluble minerals can occur in microsystems that are distal and/or proximal to the meteoric water source or conduit (Meunier et al., 2007). The flushing of fluids can also disrupt the alteration process, increasing the fluids aggressiveness at that time. Residence times of fluids in aquifers can potentially vary both spatially and temporally in short distances and times. Therefore, we will focus on the residence times of fluids that have moved from the conduit to the surrounding matrix due to reversal of the hydraulic gradient.

Screaton et al. (2004) and Mecchia et al. (2019) have used different methods to identify the residence times of recharging and discharging fluids in karst and sandstone aquifers, respectively. Both identify the infiltration of preferential flow along the conduit wall in the direction perpendicular to fluid flow, propagating until it reaches unweathered bedrock. Screaton et al. (2004) observed the loss of flow in the conduit to its surrounding non-recrystallized and high porosity limestone matrix. Using temperature, discharge, and specific conductivity values as tracers, they monitored the hydraulic pulse of fresh meteoric fluid during storm events. Based on discharge and specific conductivity values collected at these sites, the authors identified that the location where fluids resurfaced had a higher discharge than the discharge into the sink (Screaton et al., 2004). Observing this temporal lag in discharge and calculating fluid residence times, they were able to conclude that flow was lost from the conduit and gained into the surrounding matrix during periods of high hydraulic gradient. During periods of lower gradient, fluids were hypothesized to revert back into the conduit over time. High hydraulic gradients resulting

in the reversal of conduit into the matrix, purges saturated fluids out of the previously occupied surrounding matrix and into the deeper aquifer(Mecchia et al., 2019). This enlarges the diameter of chemically aggressive fluids around the conduit. The study demonstrated that fluid residence time was highly dependent on the ability for water to be retained in the matrix surrounding the conduit, which is related to the lithological characteristics of the matrix. Filipponi et al. (2009) modeled the gain of saturated fluids (with respect to [SiO_2]) into an under saturated fluid filled conduit. The saturated fluids originated from the intergranular porosity of the surrounding arenite sandstone. The concentration of the solute ([SiO_2]) was modeled to be low, resembling a preferential pathway under non-equilibrium conditions(Filipponi et al., 2009). The model simulated the transport of fluids into conduits via diffusion through the intergranular pore spaces. From the model, they observed the concentration of silica to be lower (>0 mg/L) closer to the fracture (>0.01 m) and then higher further away (8 mg/L, >0.07 m). This led them to believe that the gain of fluids from the surrounding saturated matrix into the conduit resulted in the propagation of dissolution along the conduit wall(Filipponi et al., 2009). As a byproduct of dissolution in arenite sandstones, grains were also released from the conduit wall through arenization. As the conduit enlarges the fluids low in [SiO_2] propagate deeper into the rock matrix, resulting in more dissolution along intergranular pore spaces (Filipponi et al., 2009). Preferential pathways in the conduit wall determine the rate of fluid transport into the surrounding rock matrix, therefore the heterogeneity and hydraulic conductivity of the matrix surrounding a conduit influences how long fluids reside in the aquifer.

Fluid loss from the conduit to the surrounding matrix and vice versa can be retarded by heterogeneities observed in the surrounding matrix. A study numerically modeled the flow of lagrangian fluids through the surrounding matrix, identifying the effects of heterogeneities on the residence time of solutes (Robinet et al., 2008). Robinet et al. (2008) were able to determine the variation of residence time values for particles moving out of an aquifer matrix and into the conduit. They specifically looked at individual numerical models of transport through porosity gradients and coatings. The model demonstrated the importance of the depth of the coating along the fracture surface (porosity gradient) and how it related to particle residence times (Robinet et al., 2008). Porosity gradients are the coatings that align the surfaces of the fracture wall. While, residence times for the thicker porosity gradient (2.5 mm) resembled values observed when running the model with no porosity gradient, a smaller gradient thickness (0.5 mm) allowed fluids to move through the fracture wall faster obtaining a smaller residence time. Residence time for surrounding matrixes with variable size coatings (0 mm, 0.1 mm, 0.1 mm in the coating, 0.2 mm) were also quantified. Diffusion coefficient for the coating model was set at 10^{-12} m^2/s (Robinet et al., 2008). Robinet et al. (2008) observed that coatings definitely influence the residence times of particles moving into the conduit. They hypothesized, the increase in residence times resulted from the flow of fluid from the matrix being slowed by the diffusive parameters of the coating layer. Lastly, they applied the model to quantify the residence time of a fracture within the Palmottu Granite in Finland (Robinet et al., 2008). A porosity map was created for a thin section sample of the rock and residence times calculated using the numerical models. Residence time calculated for the granite was 10^{11}s compared to the equivalent homogeneous matrix

models residence time of 10^8s. Heterogeneities in the matrix surrounding the conduit can cause different residence times due to differences in the connectivity of micro pores and fractures (Robinet et al., 2008). Differences in residence times between the model and real-world analogue was concluded to be the result of the density of microfractures in the matrix. The model used micro pores to simulate diffusive flow through the coated zone while the matrix of the analogue contained more microfractures than micro pores, allowing fluids to diffuse into deeper portions of the matrix. This results in a delayed diffuse of particles from in the matrix to into the fracture (Robinet et al., 2008).

Residence times are important for identifying the amount of dissolution that can occur in the matrix surrounding the conduit (Meunier et al., 2007; Robinet et al., 2008). However, in more soluble rock the residence times are influenced by the movement of fluids between microfractures and matrixes. Microfractures are cracks (>50 micrometers) in the matrix that connect pores together elongating the aggressive fluid infiltration into the unweathered aquifer. In microfractures, solute saturation with respect to a mineral and residence time of the solute directly relate to dissolution rate (Dreybrodt, 1990a). Chemical potentials create gradients of flow where the concentrations of solutes move from high to low potentials. Preferential pathways like conduits, concentrate meteoric low chemical potential fluids during storm events. The buildup of hydraulic head causes the flow to move from the conduit to into the surrounding matrix through microfractures (Meunier et al., 2007). Microfractures offer primary pathways for meteoric fluid into the unweathered aquifer. As aggressive fluids fill the conduit, the microfractures intersect the conduit interior wall are infiltrated. Similar to conduits of the macroscale, inception horizons also concentrate groundwater flow at the microscale forming microfractures that

enlarge according to aggressive water input. However, unlike conduits, microfractures do not contain a complete throughput flowpath where water can be infiltrated and transported to a discharging location (Meunier et al., 2007). Subsequently, both open and closed systems are integrated along the microfracture aperture leading to distinct alteration zones. Meunier et al. (2007) was able to identify the individual alteration zones by indicating locations where differential dissolution-precipitation (referred to as differential weathering) reactions were occurring within microfractures. Meunier et al. (2007) attributed differential weathering inside of the microfracture, to the chemical potential differences observed along its internal length. He defined three different zones of differential weathering; the area at the entrance of the microfracture (Open system), the area located at the termini of the microfracture (Nearly closed system), and the intermediate zone. The microfracture entrance intersects the wall of the conduit offering a primary path for fluid infiltration (Meunier et al., 2007). When the conduit is flushed with meteoric fluids, the microfracture also becomes infiltrated. The microsystem reactions that occur here are the result of far-from-equilibrium conditions as the low chemical potential (aggressive) fluids rapidly infiltrate the discontinuity, the time available for dissolution is greatly reduced. At the termini of the microfracture, fluids are near-equilibrium due to low circulation through narrow pores or dead-end microfractures. Here at the near-equilibrium zone, the rate of alteration is controlled by surface reactions between fluids and mineral grains (Meunier et al., 2007). As a result, the difference in mineral concentration goes from high to low in the near equilibrium to the far-from equilibrium conditions. This difference in concentration produces a chemical potential gradient between these two systems, circulating concentration values vary between the

two. Residence time is directly related to the physio-chemical alterations of the conduit wall once the cohesive strength of the matrix is un-bonded, piping results (Meunier et al., 2007). Unfortunately, studies identifying residence times of sandstone rock range from models to more qualitative field evidence. Therefore, there is no previous data that quantitatively identifies the residence times needed for the dissolution of conduits within soluble sandstone aquifers.

3.3.4 Conduit flow velocity

Sediment transport through the subsurface requires drainage pathways large enough for sediments to pass through and sufficient velocity to transport the different grain sizes (Herman et al., 2012). Sediment transport can be broken up into three transporting mechanisms, the solute load, the suspended load, and the bedload. Grain sizes change in each load causing the velocity required to transport the sediments to also differ. The solute load is composed of ions that originate from various weathering processes. Unlike the suspended and bedload sediments, the solute load can be transported by kinetic or diffusive energies. The transport of the solute load by these processes has been discussed in the above sections and will not be discussed further. The suspended load is composed of particle sizes of silts and clays (<0.05mm). It is often difficult to initially disaggregate clusters of particles of this class, due to the particle cohesiveness between individual grains (Herman et al., 2012). These particles therefore need a substantial fluid flux to dislodge them from their depositional area. However, once these grains are entrained in the flow they remain in suspension even with lower velocities (Herman et al., 2012). Bedload transport is composed of sediments with grain sizes larger than silt, that are dragged along the bed during flow entrainment (>0.05 mm).

Sand particles fall within this category, but as its grain sizes vary two orders of magnitudes within the class (grain size 0.05 – 2 mm) it is possible for sand grains to represent the suspended and bedload during minimum flow velocity periods (Herman et al., 2012). Gravel, cobbles, and boulders represent the remaining grain sizes of the bedload portion and require substantial amounts of kinetic energy for transport through a conduit (Herman et al., 2012). Even so bedload sediment of all grain sizes may not receive enough energy for the complete entrainment into the flow. This results in the grains bouncing along the bedding surface, or saltation (Herman et al., 2012). For a sandstone pseudokarst, the focus will be on the necessary velocity values needed to entrain particles of fine sand sizes or smaller.

In order to maintain a continual formation of pseudokarst structures, a net loss of sediment along the conduit must be maintained. Fluid transport into and over aquifers where karst and karst-like landscapes are present often brings various magnitudes of sediment into the drainage basin (Herman et al., 2012). These sediments can originate from insoluble clastic rock degradation, soil wash downs, sinkhole plug injections, and other allogeneic or autogenic sources. In locations where surficial fluid transports cannot be observed, fluids must be transported through subcutaneous conduits (Herman et al., 2012). The continual accumulation of sediment in the conduit without a greater level of erosion will result in the clogging of the conduit, preventing any further removal of aquifer mass. An aquifer containing insoluble sediments must be able to efficiently remove sediment at a rate faster than sediment is deposited within it to continue to develop pseudokarst (Herman et al., 2012). Sandstone's grain size distribution is highly dependent on its depositional environment controlling what velocity is needed to

mobilize the sediments. For example, alluvium deposits often contain very poor to poorly sorted grain distributions, deviating almost 1 to 2 standard deviations from the mean grain size (Glaister et al., 1974). As flow velocities are often episodic, larger grains can be transported through the conduit at high flux velocities and vice versa during lower velocities. Eogenetic aquifers containing near surface water tables, often have both high and low fluxes of fluids throughout the year, providing the conduit with variable velocities (Worthington, 2015). During storm events, high velocity fluids dislodge and transport the larger grains about the conduit limiting the movement of finer sediment to the area just above the bedding surface (Ghoshal et al., 2014; Herman et al., 2012). These grains are more likely from allogeneic sources due to the slow rate of dissolution and grain release when compared with the rate of sediment transport (Herman et al., 2012). As the flux decreases, the rate of dissolution of soluble material can release insoluble grains from the conduit wall allowing them to be entrained and transported in the slower moving flow. Ultimately, grain size distribution and flow velocity determine if a sediment will be transported (Herman et al., 2012).

Quantifying the controls on sediment detachment and subsequent transport in conduits and soil pipes, has proved to be difficult (Herman et al., 2012; White, 2002; Wilson et al., 2018). Some of the complexities encountered in the literature include, the collection of suspended load and bedload composition data, differentiating suspended load and bedload data, estimating variable conduit/pipe diameters, and the collection of data during storm events (Herman et al., 2012). Many papers have yet to define the mechanistic characteristics controlling sediment detachment and/or sediment transports within conduits/pipes (Herman et al., 2012; Stoeber, 2005; Wilson et al., 2016; Wilson et

al., 2018). While laboratory and modeling experiments have difficulty recreating the conditions of the natural world, observations from the field have offered insight into the aspects controlling sediment transport in conduits/pipes (Wilson et al., 2016). Velocity measurements extracted from tracer test conducted in soils and pipes have allowed for some understanding of potential flow values. For carbonate karst, velocity values within conduits represent a log-normal distribution ranging from 0.001-1 m/s, with a median of 0.022 m/s and a geometric mean of 0.020 m/s (Ford and Williams, 2013; Herman et al., 2012; Worthington, 2015). In soils, pipe flow velocities also represent a log-normal distribution ranging from 0.0005 – 0.66 m/s, with a median of 0.007 and a geometric mean of 0.061 (Anderson et al., 2009; Wilson et al., 2016; Wilson et al., 2018). Higher velocity measurements obtained from tracer tests in soils are representative of initial pipe flow velocities, which have been observed to initiate the piping of soil grains. Grains of <2 mm represent particle sizes found in alluvium deposits. At a velocity of 0.35 m/s grains smaller than <0.25 mm can be entrained in the fluid flow (Stoeber, 2005). Once silt and clay particles are suspended they remain suspended due to the upward forces caused by the turbulence of moving fluids, this is regarded as the suspended load (Herman et al., 2012). Due to the collection of mostly suspended load data in the field, it has been difficult to precisely quantify the velocity values needed to move sediments larger than those being transported in the suspended load. This lack of knowledge leaves a gap in quantitative data when it comes to the competence of the fluid moving through the conduit during bedload transport periods, resulting in the transport values of bedload materials often being estimated or approximated rather than verified in the field (Herman et al., 2012). For example, estimated velocities for the transport of sand and gravel sized

particles (>0.25 mm) are in the range of tenths of a meter per second (Herman et al., 2012). For piping to occur the velocity of fluid flow within conduit must exceed the particles resistance to flow. Based on the current literature, the minimum value for the transport of silt-fine sand particles is around 0.35 m/s (Anderson et al., 2009; Wilson et al., 2016; Worthington, 2015).

3.3.5 Lithological Factors

The development of inception horizons within an aquifer is highly dependent on how the alteration of primary porosity changes permeability of the sediments (Filipponi et al., 2009). Initially, when alluvium sandstone – siltstone complexes are first deposited, the sand and silt grains are unconsolidated. Over time, the digenesis of the aquifer results in both the removal and addition of porosity within the sediments. The initial deposition of sediment grains creates the primary porosity observed in the aquifer (Worden and Burley, 2003). As groundwater percolates through the aquifer, various sizes of allogenic sediments can become entrained in the fluid. Available porosities fill with authigenic sediment, reducing the porosity and permeability of the aquifer, and altering flow pathways at these locations (Walker et al., 1978). Flow paths can be further modified by the chemical dissolution and replacement of detrital sediments within the aquifer(Walker et al., 1978). Detrital grains such as feldspars, amphiboles, and micas represent framework grains that are thermodynamically unstable at near surface conditions (Walker et al., 1978). Unstable framework minerals undergo various chemical weathering reactions in order to reach equilibrium with interstitial aquifer fluids. Chemical dissolution and replacement of these sediments increase porosity at the reaction locations, releasing some or all of the elements contained in the altered grains into the interstitial

groundwater (Walker et al., 1978). Released elements can then be transported through the aquifer and removed from solution, or precipitated, as authigenic minerals that are stable under the current interstitial flow condition. The precipitation of authigenic minerals like, polycrystalline quartz, mineral overgrowths, carbonates, oxides including iron oxides, and various clay minerals can cement detrital grains together removing porosity and strengthening the cohesive structure of the aquifer (Walker et al., 1978). Authigenic minerals precipitate under stable chemical equilibrium conditions; however, the precipitated mineral becomes unstable once interstitial fluids deviate from the chemical concentrations that caused its precipitation (Walker et al., 1978). Meteoric fluids migrating through eogenetic aquifers can then dissolve the unstable detrital and authigenic minerals reestablishing porosity within the aquifer (Walker et al., 1978). Thin section analysis can help to delineate identify how chemical alteration has influenced the chemical aspect of pseudokarst formation (Walker et al., 1978).

The quantification of grain size variability, void spaces, and grain and cement compositions within a thin section can help to delineate if alteration has occurred in the local subsurface area (Shanmugam and Higgins, 1988; Walker et al., 1978). Modern alluvium sediments are initially deposited with a range of clay to sand. The removal of framework grains can reduce grain size variability within the altered sediment, resulting in a more sorted sample (Walker et al., 1978). A comparative analysis of grain size variability in altered and unaltered ancient sediments can help to validate the occurrence of framework grain dissolution (Walker et al., 1978). Void spaces that once inhabited unstable framework sediments, may also remain intact depending on if the aquifer has undergone any additional compaction (Shanmugam and Higgins, 1988). If dissolution

locations have been maintained, a quantification of porosity in the altered sediment compared to the unaltered sediment can provide further insight on the occurrence of diagenetic processes in the aquifer (Walker et al., 1978). Difficulty may arise when identifying porosity changes due to the readjustment of grains, to newly created void spaces. Grain readjustment result in a change in depositional texture, leading to reductions in local porosity (Walker et al., 1978). Observations of porosity without correctly identifying the engendering processes, can lead to erroneous interpretations about the aquifers diagenetic history (Shanmugam and Higgins, 1988). Deciphering how the current diagenetic processes influence the aquifer structure is pivotal in identifying the process currently influencing chemical arenization (Walker et al., 1978). Framework grain dissolution can completely remove the existence of a particular grain, turning the heterogeneous sediment to a more homogenous composition (Shanmugam and Higgins, 1988; Walker et al., 1978). Incongruent dissolution of framework grains commonly occurs during diagenesis, therefore, a comparison of sediment compositions between altered and unaltered samples can help to avoid misinterpretations of diagenetic history (Walker et al., 1978). In alluvium sediments, this comparison has been observed to result in an increase of quartz grain components in more altered sediments, representing a more mineralogically mature sample (Walker et al., 1978).

The physiochemical reactions of framework grains and authigenic minerals control permeability in various ways. In the early stages of framework grain dissolution, major dissolution of framework grains follows already established permeability pathways (Shanmugam and Higgins, 1988). Initially, partial dissolution of framework grains creates disconnected void spaces, making it difficult for fluids to migrate along a

particular path (Shanmugam and Higgins, 1988). Continual dissolution of framework grains around the newly created void, provides a better connection between disconnected pores (Siebert et al., 1984). Once a primary connection is established, meteoric fluids can percolate through the aquifer increasing permeability 2 - 3 orders of magnitude (Shanmugam and Higgins, 1988). Thin section analysis of void space size along a particular horizon can help to identify if a connection between pore spaces was established and how unstable minerals aided in formation of the pathway (Shanmugam and Higgins, 1988).

Where fluids are chemically oversaturated and kinetics allow precipitation, authigenic minerals form. In sandstones, the authigenic mineral cements the quartz grains together. Authigenic cements form in different locations, surrounding pores or filling pore spaces (Walker et al., 1978). The location of the mineral precipitation greatly influences the permeability of the sample (Worden et al., 1998). For example, in the Chatomy Formation sandstone (Paris Basin), quartz cement was less pervasive than dolomite cement and resulted in a permeability of two orders of magnitude difference for samples with similar porosity (Worden and Matray, 1998). This permeability difference was due to dolomite cement filling pores and blocking pore throats, degrading permeability at a greater rate than quartz overgrowths. Authigenic mineral response to fluid infiltration also influences permeability (Walker et al., 1978). For example, a computer simulation model noted that samples coated with swelling clays reduced permeability almost 10-40 % when compared to uncoated samples (Aksu et al., 2015). The same study also demonstrated that smaller grain sizes (0.105-0.210 mm) compared to larger grain size (0.707-0.841 mm) increased the influence of swelling clays on

permeability reduction. They stated that a decrease in pore space size causes a more profound response to clay swelling. In thin section, speculation from voids created by dissolved framework grains can be constrained by the formation of authigenic cements (Aksu et al., 2015). Removal of these cements at periods of disequilibrium leads to changes in permeability, potentially helping to facilitate arenization and pseudokarst formation. Therefore, it is important to identify the results of diagenesis that may contribute to porosity and permeability alteration in sandstone rock (Walker et al., 1978; Worden and Burley, 2003). Karst landscapes contain particular geological, geophysical, hydrological, geochemical, and biological parameters that help lead to further the dissolution of the aquifer. To understand how parameter values influence formation of karst, each factor must be quantified. This has been done for many karst structures throughout the world, however, an understanding of how similar parameters control pseudokarst formation, has yet to be established (Wray and Sauro, 2017). Karst formation is highly dependent on the above parameters as they help present the environment where adequate dissolution can occur. In the pseudokarst environment these factors are just as important, as they help manage the balance between the dominating processes in arenization (Wray and Sauro, 2017). Therefore, it is necessary to define how the literature has quantified each parameter in karst rock so that similar quantifications can take place in this survey.

3.3.6 Geological Controls

For landscapes to be termed “karst” dissolution of soluble species must be the main cause of deformation within the aquifer (Ford and Williams, 2013). The dissolution of aquifer minerals takes place in locations where groundwater can reach the soluble

species. This normally occurs along inception horizons where bedding and fracture planes create enough space for the transport of groundwater fluids. Dissolution rates of common pure minerals have been identified in labs however, in natural environments dissolution rate is based on a combination of different parameters (Ford and Williams, 2013). For example, the dissolution rate of a pure feldspar minerals measured in the lab, is 5 times faster than feldspar dissolution calculated from in situ mass balance equations at similar pH and temperature (Zhu, 2005). Although, laboratory environments provide a controlled environment for the deduction of dissolution rates, using laboratory data to assess the natural world produces many difficulties. This is due to spatial heterogeneities within the aquifer and a misunderstanding of how the heterogeneities are influenced by the hydrological and chemical parameters applied to the aquifer (Worden and Burley, 2003). This is especially true in sandstones where the aquifer may contain various compositions of sand sized particles that influence how well the sandstone dissolves. Although most sandstones contain quartz, they also contain other detrital and authigenic grains and cements like feldspars and calcites that more susceptible to dissolution than quartz. Laboratory dissolution rates for quartz (10^{-19} mol/m^{2}s) demonstrate the relative insolubility of quartz crystals, placing the mineral at almost 10 magnitudes times less dissolvable than feldspars (10^{-5} – 10^{-12} mol/m^{2}s) and calcites (10^{-10} mol/m^{2}s) (Palandri et al., 2004; Wray and Sauro, 2017). Sandstones containing soluble mineral constituents can lead to the formation of secondary porosities, in fact a porosity enhancement of 30 % is all that is needed to initiate pseudokarst development (Mecchia and Piccini, 1999). Therefore, identifying locations where dissolution may have happened as well as grains

that may be susceptible to dissolution can help to better understand the effect geology has on pseudokarst formation.

3.6 Lines of Evidence for Hydrologic Controls on Pseudokarst Formation in a Field Setting

This section will describe the lines of evidence to identify the hydrologic controls of pseudokarst occurrence in a field setting using geophysical, hydrological, geochemical, and biological aspects.

3.6.1 Geophysical

Subcutaneous inception horizons like fractures and joints, provide high permeability pathways for groundwater to migrate through the aquifer (Filipponi et al., 2009; Marco and Pierre-Yves, 2008; Mecchia et al., 2019; Sauro, 2014; Wray and Sauro, 2017). Along these pathways occurs the majority of dissolution processes. Without inception horizons the formation of karst landforms would not be possible. Similarly, in pseudokarst, the presence of inception horizons help pave the way for dissolution and piping of aquifer materials (Mecchia et al., 2019; Sauro, 2014; Wray and Sauro, 2017). Therefore, identifying the presence of inception horizons in the subsurface environment is imperative for demonstrating active karst or pseudokarst development. However, difficulty arises when it comes to identifying structures in the subsurface. Geophysical surveys provide a noninvasive look into the subsurface geology. Due to the ambiguity encountered while conducting geophysical surveys, most studies either use geophysical techniques complimentary to one another or provide ground truth samplings to verify survey results (Doolittle 1998, Wightman 2008, Yawar 2020).

In some environments electrical resistivity imaging (ERI) has proven to be an advantageous surveying technique for identifying karst structures, such as sinkholes, that develop from dissolution and piping (Greer et al., 2017; Hussain et al., 2020; Ismail et al., 2012; Ramakrishna, 2011; Rayner et al., 2007). The sole use of one geophysical technique can cause ambiguous results due to the limitations encountered in each technique. For example, ERI resolution is highly dependent on the scale of the survey meaning that only if the scale is selected correctly can the subsurface accurately be delineated (Ramakrishna, 2011). Studies have used temporal ERI to identify hydrologic flow of fluids (Greer et al., 2017), zones of fractures and stratigraphic layers (Rayner et al., 2007), and subsurface voids (Ismail and Anderson, 2012), many of which have used ground truth data to verify results. To reduce ambiguity of the ERI results, data from ground truths or other geophysical techniques can be collected. The ground-truthing of geologic data permits the correlation of coring to layering observed in the ERI. Spatial variances of stratigraphic horizons cause interpretations to vary slightly according to the extraction locations. The use of ground penetrating radar, GPR, with ERI has demonstrated to be a powerful verification combination (Hussain et al., 2020). Resolution limitations arise in GPR data when the radar signal becomes attenuated upon entering the subsurface. This can occur in clay or similar materials that cause scattering of the signal making it difficult to image below the attenuating stratigraphy (Hussain et al., 2020). Ultimately, no geophysical method is perfect and all have their own limitations. The correct selection of geophysical method(s) is imperative in order to correctly asses the location of subsurface alteration.

3.6.2 Hydrological

In karst environments the hydrologic response to precipitation events both big and small, result in unique variances in water table and fluid discharge values (Barbel-Périneau et al., 2019; Florea et al., 2006; Halihan et al., 1998b; Kovács, 2003; Li et al., 2020; Martin et al., 1999; Martin and Dean, 2001; Moore et al., 2010; Williams, 1983). These variations can be observed in hydrographs and broken into two parts; P1, representing the pronounced peaks of the hydrograph demonstrating rapid inflow and outflow of meteoric fluids that indicate a good surface connection to conduit locations, and P2, representing the smooth traditional recession shape of the hydrograph. Peaks are controlled by how well fluids move through preferential pathways in the aquifer. When preferential pathways contain a constriction, flow within the conduit is slowed resulting in water ponding upstream from the constriction into the epiphreatic passage, an increase in the hydraulic gradient, and an increase of the velocity of flow (Halihan et al., 1998b). Constrictions such as these have been observed in hydrologic data collected above constrictions to result in the increase of the water table 5-10m from its baseflow elevation. Conversely, during these periods flow observed downstream from the constriction only fluctuated >1m (Halihan et al., 1998b).

Once the hydraulic pulse moves through the constricted area, the water begins to subside returning to its baseflow position. The rate at which the aquifer drains is also an important identifier of constriction flow, as it demonstrates that the aquifer drains at different rates depending the routes of drainage (White, 2002). Fluids filling the conduit drain faster than fluids draining from the surrounding aquifer matrix. In karst aquifers the quantification of drainage times or recession coefficients have been able to describe the

different flow regimes within karst aquifers (Kovács, 2003). Recession coefficients are found from plotting discharge or hydraulic head vs time in a log-normal graph and obtaining the slope, or recession coefficient in 1/s (Kovács et al., 2015). The analytical solution for the shape of the hydrograph demonstrates that different recession coefficient slopes can be representative of more than one particular flow regime (Kovács et al., 2008). White (2002) suggested that these regimes may be representative of flow draining from the conduits (quick flow) and flow draining from the fractures into the conduit (slow flow). Observing water level rises, relatively large hydraulic gradient changes, and multiple recession coefficient values within a hydrograph are indicative of differing draining rates (White, 2002). Under the right conditions fluid pulses that cause the reversal of flow into the conduits may permit aggressive fluids a longer time inside of the aquifer surrounding the matrix, leading to more dissolution.

3.6.3 Geochemical

Spatial changes in fluid geochemistry are indicative of recharge, discharge, water-rock reactions. Not only does this information help to delineate chemical reactions, but it can also help to identify fluid residence time in the aquifer. Equally as important as the fluid chemistry, residence time permits the fluid rock interaction with time to perform the necessary reactions. Measurements of residence times often use trace elements to measure aquifer residence times. Environmental tracers such as temperature, pH, EC have been used to estimate fluid residence times and predict groundwater velocity in karst aquifers (Martin and Dean, 1999). When storm pulses move through the aquifer, environmental tracers provide initial parameters for the analysis of temporal change. Many studies have identified dissolution as the primary control in the formation in karst

and karst like landscapes, however in sandstones the potential lack of soluble spices and variability of permeability may result in dissolution not being of primary importance in arenization of sandstone (Dreybrodt, 1990b; Dubois et al., 2014; Ford and Williams, 2013; Halliday, 2007; Martini, 1979; McBride, 1989; Mecchia and Piccini, 1999; Mecchia et al., 2019; Sauro, 2014; Wray and Sauro, 2017). Monitoring the environmental tracers and the release of major ions into the groundwater will help to identify what reactions are dominating the sandstone subsurface. Current karst studies use a stochastic approach to identify water-rock weathering potential, rock types involved in chemical reactions, and the direction of equilibrium reactions in the subsurface (Bandstra et al., 2008; Barbel-Périneau et al., 2019; Datta and Tyagi, 1996; Gibbs, 1970; Katz et al., 1998; Meng et al., 2016). However, an in-depth geochemical survey is beyond the scope of this thesis. Observing how environmental tracer values change in accordance with fluid chemistry can provide a better understanding on what reactions are occurring in the subsurface.

3.6.4 Biological

The alteration of an aquifer is not limited to abiotic processes, like chemical and mechanical weathering, but can also be facilitated by microbial growth. For microbes to thrive they require nutrients for energy production, substrate to live on, and water (Atekwana et al., 2006). As there are rarely any changes in the amount of available nutrients beneath soil layers at the bedrock interface, most microbial growth is restricted to shallow regions. However, as of recently, anthropogenic influences have permitted the growth of microbes to beyond this horizon (Atekwana et al., 2006). As a result, much of today's literature reflects microbial environments originating from anthropogenic

influences rather than the microbial environments response to natural subsurface conditions (Atekwana et al., 2006). Nonetheless, the alteration of karst aquifers has been observed to occur as the result of biogeochemical mechanisms. These mechanisms include, microbial growth on rock surfaces or crevices resulting in corrosion, erosion, grain borings, the increase of superficial denudation area through the growth of microbial denudation mats, intensification of weathering by organic acids and the production of CO2 by microbes during respiration on the rock surface, and the production of biochemical ligands by microbial nutrient uptake causing the release of mineral elements from the rock surface (Bin et al., 2008). When microbes are provided aspects of microbial growth in strata that's deeper than the soil layers, they can grow on any surface. However, in the sandstone pseudokarst literature very few studies focus on the influence of microbes on arenization and thus no clear evidence has been published on this topic (Wray and Sauro, 2017).

Electrical resistivity Imaging has proved a vital tool in identifying the presence of potential microbes in the subsurface. As microbes consume nutrients and thrive on substrates, they produce microbial mats that help electrons migrate from one location to another (Atekwana et al., 2006). Cation exchange between microbes living in the mats, their substrate, and surrounding pore spaces leads to a temporal variability in ionic content of the subsurface (Atekwana et al., 2006). The presence of microbial growth can be observed using temporal electrical resistivity imagery. In studies where anthropogenic contaminants were present, providing nutrients to microbes in the subsurface, electrical conductivity measurements demonstrated 2-6 fold increases compared to background images taken, (Atekwana et al., 2006; Che-Alota et al., 2009; Sauck, 1998). Temporal

conductivity measurements using ERI technology can be beneficial in identifying zones of microbial growth, however delineating how microbes are altering the subsurface is a difficult task. According to previous published results, the delineation of microbial degradation processes requires the analysis of environment of degradation, isolation and extraction of microbes, benchtop microcosm experiments, and verification of process in the field (Chakraborty et al., 2012; Kästner et al., 2010; Thullner et al., 2009; Utom et al., 2019). Therefore, this study will only delineate the presence of microbes through analysis of conductivity values within the ER image.

CHAPTER IV

4.0 METHODOLOGY

Several methods were utilized to obtain field data at the Lightning Lake Research Site to evaluate the distribution and causes of pseudokarst features. Field data collection methods are described in this order: land survey data, geophysical data, hydrological data and lithological data. This is followed by data analysis techniques applied to above data.

4.1 Land Survey Data

Field site coordinates for site features were quantified using a Leica differential GPS (REF to Leica model). Pseudokarst features mapped during this study include gullies and sinkholes. Hydrological sampling locations included a hand dug well, on-site springs, and Lightning Lake. Geophysical data acquisition locations include the spatial extents and electrode locations of individual ERI lines. Spatial data were collected at 0.3 centimeter resolution. When vegetation was too thick for good GPS data, optical surveying equipment was used to fill in any data gaps for elevation data beneath trees. The GPS data were suitable for easting and northing coordinates in the wooded areas.

4.2 Geophysical Data

Electrical resistivity data were collected using a Supersting eight channel resistivity instrument from Advanced Geosciences, Inc (AGI). A total of nine electrical resistivity images (ERI) and one temporal ERI (TERI) image were collected during the study period. Lines were spaced methodically to identify areas of hypothesized groundwater flow and provide a three-dimensional perspective of the site. The selected locations were also based on proximity to psuedokarst structures (sinkholes, gully valleys, springs etc.) that were indicative of the removal of subsurface mass. The ERI surveys utilized either 28 or 56 electrodes spaced 1-3 m apart from each other and ranging from 55-165 m in total line length. The length of the ERI line depended on the intended depth as well as the lateral available space on the property. The imaging depth associated with each line is approximately equal to one fifth of the total length of the line. For example, the 55 m line will image approximately 11 m deep. The instrument was powered by a 12V power supply box with an external 110V gasoline powered generator. A contact resistance test was performed for each line to ensure a good electrical connection between the electrode and the surrounding sediment/material. A contact resistance of less than 2,000 Ohms was considered suitable. High contact resistance electrodes were pounded deeper into the subsurface or salt water was added at the electrode to reduce the initial contact resistance. The temporal datasets were collected before and after a storm event. Temporal surveys help to identify changes in conductivity by comparing resistivity data at two times. The datasets were acquired and processed using the Halihan/Fenstemaker method (Halihan et al., 2005; Halihan et al., 2020).

4.3 Hydrological Data

The site contains a lake, a hand dug well, and a piezometer in the fault zone. A barometric pressure transducer (Solinst) was placed adjacent to the lake. Water level pressure transducers (Solinst) and electrical conductivity (EC) transducers (Onset) were placed in both the lake and the hand dug well at the site. Transducers collected temporal data at 15-minute intervals and were downloaded every 2 months. A 3" piezometer was hand installed in the center of the gully downstream from the horizontal well based off a comparison of land survey data (Figure 2.2). The entire interval was silty clay material that was dry for the majority of the depth. Depth of the piezometer was approximately 5 m which is at least 3 m below the lake elevation with a 0.3 m screened interval. The piezometer was periodically checked for water after storm events but ultimately yielded no water.

Hydrologic data were collected from June 2019 to September 2019. Barometric pressure corrections adjusted the raw transducer data by +/- 0.01 - 0.11 meters. During the measurement period, a total of three large and one small storm events occurred. Data from each storm were used to quantify hydraulic gradient, providing data for how fluids move through the aquifer. EC and temperature data were collected and compared to the barometrically corrected hydrologic data to identify when the storm pulse reached the hand dug well. Due to instrument error, only hydrologic data from the hand dug well after 8/23 was used to create the EC and temperature graph.

Groundwater in the hand dug well was pumped to identify the location of flow features within the well. While pumping at 1.9 liters per second (25 gallons per minute), the well-drained completely in approximately one hour. During pumping, the author

repelled to the base of the well to note change in lithology and recharge zones following confined space protocols. The majority of the well walls only had mild seeping into the well. The major recharge feature was a fracture observed at the base of the well in the siltstone interval at approximately 294 m amsl. The elevation of the dominant fracture zone was recorded and compared with data from the geophysical survey.

4.4 Lithologic Data

Lithologic samples were also extracted from the site to delineate the permeability of sampled sediment. Samples were taken from inside within the gully valley using a hand auger during the installation of the piezometer. The hand auger was inserted and a hammer was used on top of the auger to allow for the collection of an undisturbed sample. Data from the ERI line 07132C provided a hypothesized elevation of the water table, which was 288 m AMSL. Undisturbed samples from the gully valley were evaluated for permeability using an Eijkelkamp laboratory permeameter (Eijkelkamp, 2013).

4.5 Data processing and analysis

GEOPHYSICAL DATA ANALYSIS

Data points collected from the Leica GPS for ERI lines were recorded and transferred into a spreadsheet. The values were then evaluated on the continuity and fluctuations of easting, northing, and elevation data as some lines went into heavy vegetation increasing the spatial error. This was done by plotting easting and northing data in Excel and fitting the points to a trend line for the ERI lines in the field. If surface line data did not achieve r-squared values greater than 0.80, the anomalous points were removed until it was achieved as the lines were known to be straight. Miscalculation of

elevation data due to the interference of trees blocking the satellite signal creates inaccurate values that must be corrected to accurately describe the topography. To mitigate this error, topography was plotted in excel to observe any discrepancies due to GPS error under trees. Where applicable, elevation data were corrected and adjusted to the WGS84 datum.

Land survey data were interpolated with processed ERI data to delineate the extent of lithological layers exposed at the surface and in the hand dug well. Locations of interest, water table elevation, and bedding plane elevations were imposed onto the processed ERI images. The temporal ERI dataset was then processed to identify locations where a conductive change in magnitude had occurred. These elevations were roughly horizontal across the dataset and assumed to be bedding planes. Both bedding planes delineated from land survey and temporal ERI provided potential flow path elevations and were imposed onto other ERI lines to identify if any connection existed between them and low permeability zones.

HYDROLOGIC DATA ANALYSIS

Upon extraction of transducers the water level in the well was measured from the top of casing to calibrate measurements from the transducer. The raw continuous dataset was plotted against time to identify trends in water table elevation. Any data points that exhibited an unnatural rise or fall in water table height (>50cm in less than 15 minutes) was removed from the data file. Once the anomalous data was removed, water level fluctuations between the hand dug well and dock were compared to demonstrate their disproportionate responses to storm water infiltration throughout the entire study period. Data collected from the electrical conductivity transducer was then graphed against

temperature and water level to demonstrate how all responded to an influx pulse of fluids. Next, hydraulic gradient was calculated for the entire data set using equation 1, where *h* and *L* are the hydraulic head and distance between the hand dug well and the dock transducer location. Lastly, the deceleration of ground water flow out of the aquifer was calculated for the recession period of 06/06/19-07/20/21. Values were calculated by plotting the water level against the day then fitting a trend line to the graph. Once the trend line was established the equation of a line was found and the second derivative was then calculated. Time was then plugged in for the second derivative and the deceleration of fluids draining out of the aquifer was determined.

LITHOLGICAL DATA ANALYSIS

Lab analysis was undertaken with competent samples collected from the gully, to quantify its hydraulic conductivity. These samples were processed using an Eijkelkamp laboratory permeameter. Permeameter values are determined using calculations originating from the constant and falling head methods. Using the method described in Eijkelkamp (2013), hydraulic conductivity was able to be determined from sediment collected in an aluminum cylinder.

CHAPTER V

RESULTS

In this section we will discuss the results of the study. This section will be ordered as follows; land survey data; geophysical data; hydrologic data; and lithological data.

5.1 Land Survey Data

Unlike traditional karst blind valleys that develop where soluble rock meets an insoluble lower bedding surface (Ford and Williams, 2013), this valley occurs within a low solubility sandstone structure with the top of the valley consisting of sandstone and the bottom is siltstone (Figure 5.2). The locations of gullies based on elevation changes tend to be over the upper portion of the siltstone in the middle of the valley (Figure 2.1). Elevation changes within the gully in this study range from 299 m amsl at the top northern side to 291m amsl at the southern base of the gully near the lake. Lake elevation often varies according to how intense the rainy season is, but values normally fluctuate around 290 m amsl as the lake level is controlled by a dam with an outlet pipe and a spillway. Transducer locations are located at the hand dug well and the dock at about 294m and 289m amsl respectively (Figure 5.2). The base of the excavated portion of the hand dug well is about 5m below the top of the well casing (approximately 294m amsl). Two distinct beds occur in the hand dug well. The first, a sandstone extending from the

surface to 3 m depth (296-299 m amsl), and the second, a siltstone layering extending to the base of the well (below 296 m amsl). Flow from the well mainly discharged from a large bedding plane at the base of the well at an elevation of 294 m amsl. Spatially, the land surface of the hand dug well is 74 m away from the dock and 9 m higher in elevation. A piezometer within the gully axis (Figure 5.2) is 292 m asml at the land surface and approximately 5 m deep (~287 m amsl).

Sinkholes are mapped throughout the study site (Figures 2.1 and 5.2). They are six inches wide and about a one foot deep. They are located between +/- 1 meter above the 295 m AMSL elevation. Additionally, the sinkholes are only present where elevation decreases from 295m to 290 m amsl within 25 m.

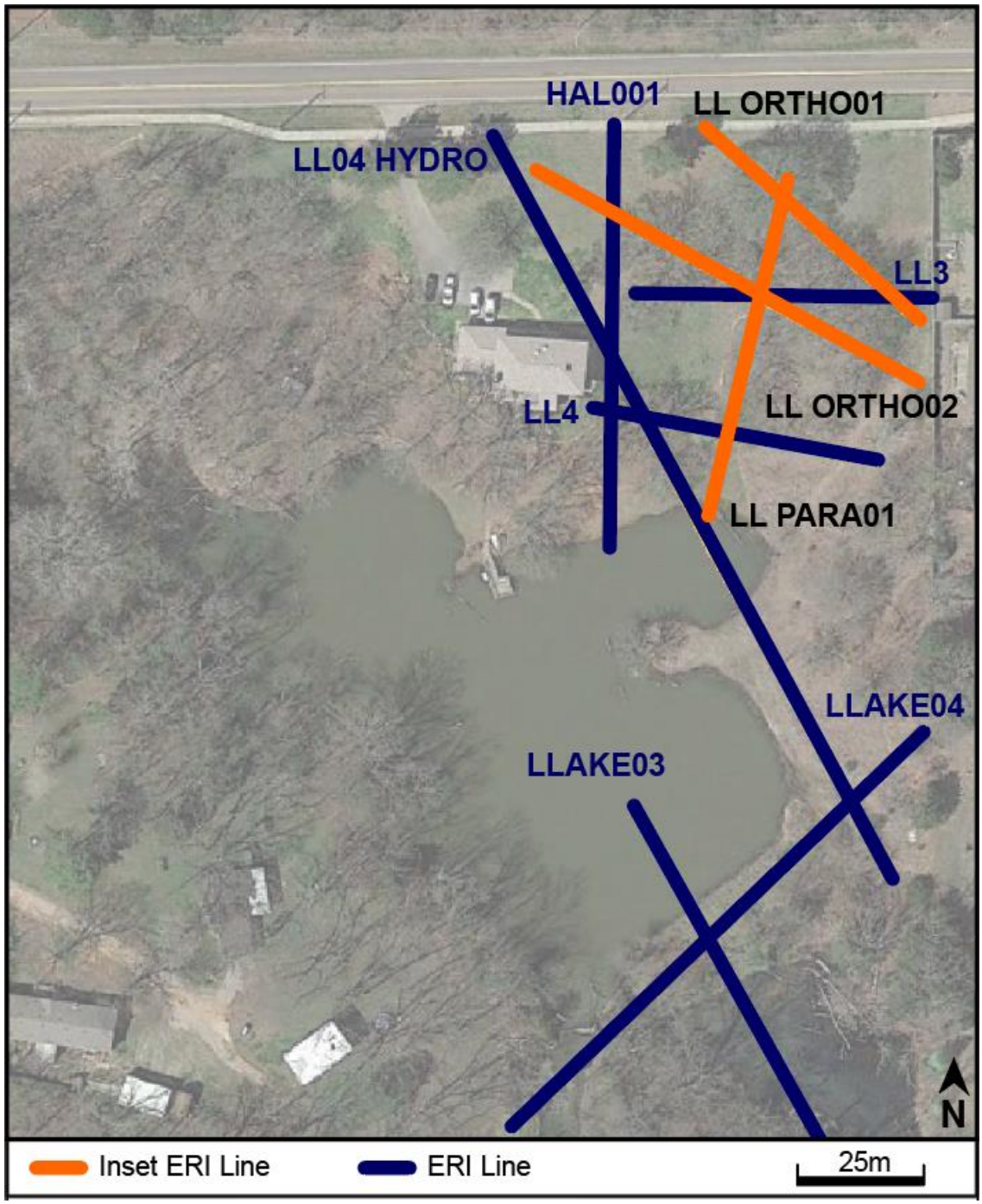

Figure 5. 1 Overview of ERI images taken. The lines in black are the images displayed in the text (Figs 5.3, 5.4, and 5.5). Orange Lines represent other ERI lines present.

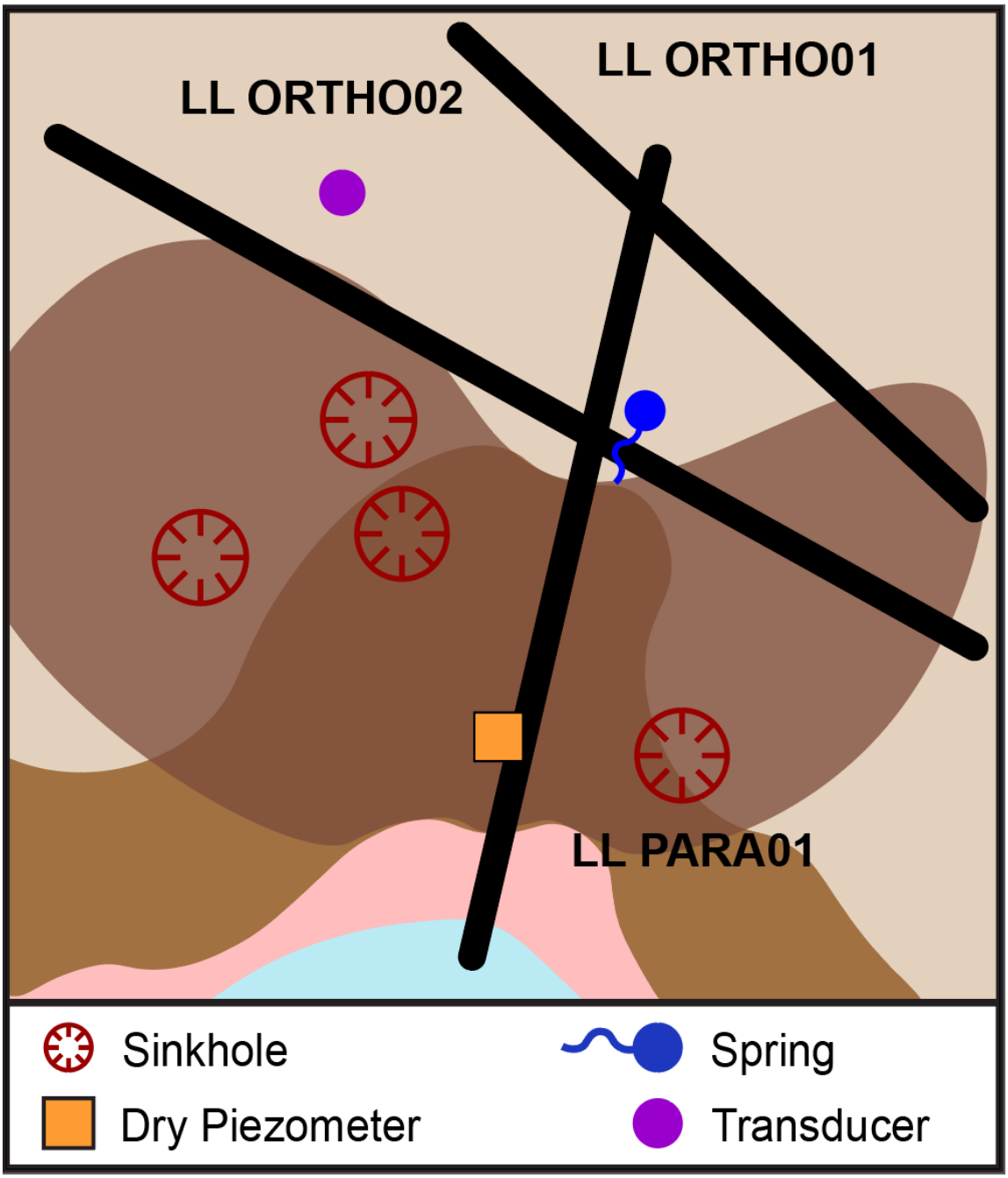

Figure 5. 2 Here is the zoomed in inset map from Figure 2.2, where Pink – Clay, Brown – Siltstone, and Tan – Sandstone. The darker brown overlying lithological layering represents the extent of underlying weathering zone observed in each ERI image

5.2 Geophysical Data

ERI lines were performed across the site (Figure 5.1). The data were of good quality with root mean square (RMS) errors ranging from 2.6% to 8.6% with an average of 5.1% for the inverted ER datasets. The site is reasonably conductive and contact resistance is low except in locations in the sandstone where additional salt solution for electrodes was needed to provide good contact. The resistivity range for the site extends from below 5 ohm-m in conductive areas and the resistive portion can extend somewhat above 100 ohm-m.

The ER datasets were able to distinguish three distinct resistivity zones, a conductive range (<10 ohm-m), a resistive range (>28 ohm-m) and an intermediate range (10-28 ohm-m). These three ranges were observed in 7 of 9 ER datasets collected during the survey. The intermediate zone is observed in all ER datasets, but the resistive range is not present where the dry upper sandstone is not present. The stratigraphic layering of the resistive zones is stable throughout the site. For example, throughout the site in areas where topography is above 296 m amsl, a resistive zone exists that corresponds with the upper sandstone unit on the site. Beneath the 296 m elevation, the resistive zone commonly grades into intermediate and conductive zones that can be observed throughout the site. Beneath the 287 m amsl elevation is another resistive zone present in all ER images where the depth of investigation reaches that depth. When correlated to rock outcrops, well stratigraphy, and gully corings of the site, these zones of resistivity represent sandstone as the most resistive, siltstone is intermediate, and clay intervals are conductive.

The results of ERI lines will be examined in further detail in the gully area that was investigated (inset map in Figure 5.1). Each individual ERI Line is displayed with the collected image as well as a conceptual model of the image beginning with LL PARA01 (Figure 5.3). This line was acquired parallel to the gully and fault. LL PARA01 illustrates the stratigraphy of the site displaying the upper sandstone, siltstone, and lower sandstone interpreted lithology (Figure 5.3a). The weathering zone within LL PARA01 is indicated by the intermediate zone of conductivity in the ERI (Figure 5.3b). The weathering zone exists mainly within the siltstone layering. In the center of the interpreted weathering zone is the conductive clay boundary, delineated by the piezometer located in the gully at 50 m laterally in the dataset. The piezometer did not leave the clay interval during installation.

ERI Line LL ORTHO01 was taken orthogonal to the gully and fault above the gully on the flat bedrock surface above Garber Ridge Spring (Figure 5.4). Within the fault zone at about 12.5 m laterally is a vertical conductive zone (< 10 ohm-m) interpreted to represent the primary fault. Surrounding the fault is a zone of intermediate resistivity, interpreted to be the fault weathering zone. The weathering zone extends from 25 m to about 40 m laterally, decreasing in vertical elevation towards the 40 m point. At 20 m in the lateral direction the height of the weathering zone reaches about 296 m amsl. Near this elevation the weathering zone juts to the left (southeast) from 20 m to approximately 12 m in the lateral direction, reaching the surface, corresponding to the location of the intermittent Garber Ridge Spring. Between an elevation of 291-294 m amsl the weathering zone breaks from the central fault zone and migrates to the left until the left side (southeast) of the dataset. This is interpreted as the siltstone boundary.

ERI Line LL ORTHO02 was also taken orthogonal to the gully and fault downgradient of the Garber Ridge Spring in the gully (Figure 5.5). This dataset did not observe the vertical conductive zone through the sandstone seen in the upgradient dataset, potentially due to significant weathering of the fault zone. A background and temporal resistivity dataset were acquired for LL ORTHO02. The background image (collected 05/04/2020) displays a conductive zone completely surrounded by intermediate zone resistivity values (Figure 5.5B). It also displays a resistive zone protruding from the bottom of the image. Before the temporal line was collected, a storm event occurred on 05/07/2020, 3 days after the background image was collected and deposited 25 mm of rain. During this storm event no fluid was discharged from the ephemeral Garber Ridge Spring. Data compared between the background and temporal imaged identified two areas of 10% conductivity changes, one being about 25 m horizontally on the dataset and the other being at 70 m towards the end of the image (Figure 5.5B and C). The other changes in conductivity occur all along a horizontal boundary at about 291 m amsl. All significant changes in electrical conductivity occur outside of the interpreted electrically conductive (< 10 ohm-m) clay pocket in the center of the fault zone (Figure 5.5C).

Flowpath Delineation

Data collected from land survey and ERI surveys was integrated and synthesized to delineate flowpaths within the survey area. Physical inception horizons indicated from the land surface and the hand dug well, offered a view into the subsurface otherwise unobserved in the ERI. During the decent into the well, bedding planes were identified at 296m and 294m amsl. The lowest bedding considered the primary inception horizon in the hand dug well location in the upgradient area of the site. These data were integrated

with the ER data by superimposing elevation location on ER datasets at the observed elevations. When correlated with the hand dug data, the weathering resistance of the sandstone and siltstone lithologies could be deciphered. In image LLORTHO01, the siltstone lithology beneath the 294m inception horizon decreases in resistance to 10-25 ohm-m (intermediate zone). However, in the same image, the intermediate zone abruptly stops after about 22m in the lateral direction. Upon the examination of the lower elevations of the ER images, we identify two additional bedding planes at 291m within the siltstone layering and 287m amsl at the sandstone/siltstone interface. The temporal image demonstrates the fluid transport capabilities of the bedding plane at 291m (Figure 5.5C). Along this bedding plane, increases in conductance (%) were observed after a storm event, therefore we interpret this bedding plane as an inception horizon where sediments can be piped during high flow events. Similar to the inception horizon at 294 m, the 291 m inception horizon can be observed to terminate the 22 m in the lateral direction within LLORTHO01. Both inception horizons are the results of fluids being concentrated along horizontal bedding planes within the siltstone lithology.

At the surface of LLORTHO01 the Garber Ridge Spring discharges fluids during large storm events. The inception horizons discussed above constitute the horizontal flow through the aquifer. However, in the ERI both inception horizons terminate at 22m in the lateral direction (Figure 5.4). In LLORTHO01, it is also observed that the intermediate zone rises into the overlying sandstone lithology at 22 m in the lateral direction. We hypothesize that this change in resistivity is the result of the ascent of fluid near the 22 m lateral boundary. Once above the sandstone-siltstone interface at 296 m amsl the

weathering zone follows the bedding plane until it reaches a discontinuity causing the Garber Ridge Spring (12 m in the lateral direction).

Clay Zone Delineation

Flow paths along the horizontal bedding plane inception horizons come in contact with the conductive layer (<10 ohm*m). The temporal ERI Line from LLORTHO02, shows that very little conductivity change occurs within the conductive zone (Figure 5.5C). In fact, the continuous conductivity change observed in the first 0-40 m in the lateral direction along the 291m amsl inception horizon, becomes discontinuous just as it reaches the contact of the conductive zone (at 40 m lateral). However, within the conductive zone a small (2-3 m) change in conductivity occurs at 50 m in the lateral direction along the 291m inception horizon (Figure 5.5C). Compared to the continuous conductivity change observed in the western portion of the image (0 – 40 m laterally), this small conductivity zone may be the result of a conduit that has been restricted in size by the conductive zone. Additionally, only after the conductive zone terminates at 62 m in the lateral direction, do we see the continuous change in conductivity along the 291 inception horizon (Figure 5.5C). Based on the ER datasets and the core at the piezometer in the gully, we hypothesize the conductive zone below 10 ohm-m to be a low permeability clay zone.

The conductive zone imaged in LL PARA01 is present from 20 m in the lateral direction to the end of the image (Figure 5.3). The dry piezometer is present in this conductive zone at 50 m in the x direction. The low permeability zone represents a horizontal lens that begins at 20 m laterally and 291 m amsl. At 27 m in the lateral direction the change in subsurface topography at the resistive boundary near the siltstone-

sandstone interface causes the conductive zone to increase to just above 291 m amsl (Figure 5.3). Once the resistive boundary decreases back to beneath 287m at 35 m in the lateral direction, the conductive zone reaches to beneath the interpreted 291 m amsl inception horizon. In LL PARA01 the weathering zone is limited to the siltstone horizon except in locations before the low permeability zone (at 20m in the lateral) or locations where the low permeability zone moves beneath the 291m inception horizon (Figure 5.3). Thus, flow paths moving along inception horizons that come in contact with the electrically conductive zones below 10 ohm-m are deflected due to the low permeability of this zone in the center of the gully.

Based on the above ER images the extent of the low permeability clay zone can be delineated. ERI LL PARA01 demonstrates the clay zone is present between lateral distances 20 – 67.5 m (Figure 5.3). In this image, from 60 to 67.5 m in the x direction, the clay layer outcrops at the surface. LL ORTHO01 (Figure 5.4) shows that the clay zone is contained between 15-20 m in the lateral direction, however LL ORTHO02 (Figure 5.5) shows that the clay boundary increases in width to about 35 m (25-60m in lateral distance). Based on ER images collected during this study, the zone of clay grows in horizontal thickness closer towards the lake, however, moving in the opposite direction the clay boundary decreases in width and stops abruptly at 20m in the x direction in image LL PARA01. These data are visualized in Figure 5.2 where the clay extent is represented as being within the weathering zone. As observed in Figures 5.2 and 5.3, the weathering zone and clay horizon only exist closer toward the lake and begin to terminate in LL PARA01 (Figure 5.3) at 20m in the x direction.

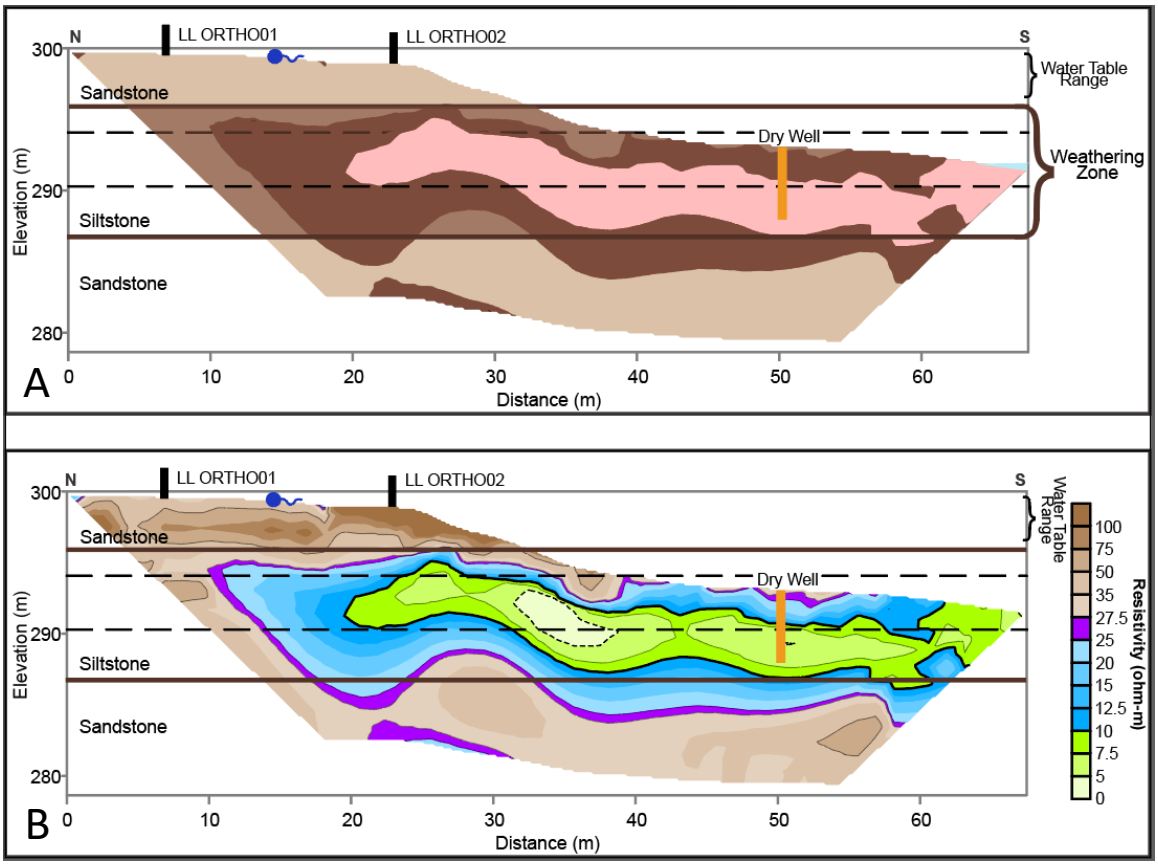

Figure 5. 3 ERI Line LL PARA01 conceptual model (A) and Electrical Image (B). Note: the weathering (intermediate conductivity) zone exists mainly within the siltstone layering; also, the range in water table in the upper sandstone and the lake level are both above the dry piezometer screened interval at the base of the well.

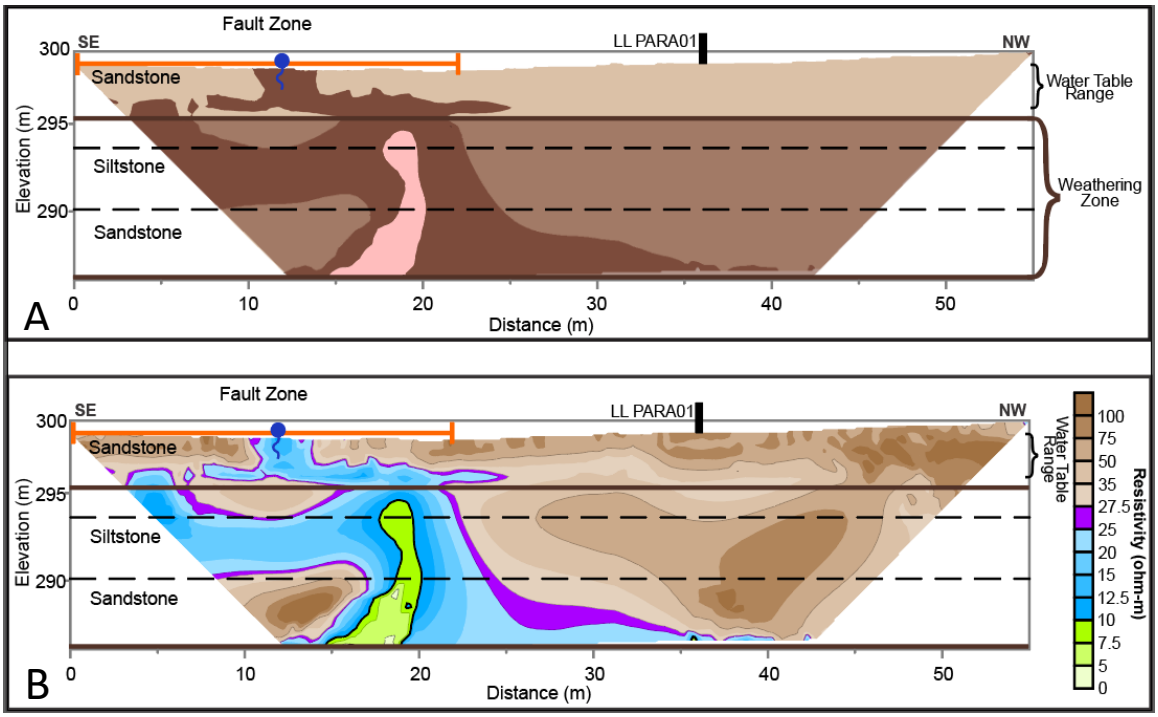

Figure 5. 4 ERI Line LL ORTHO01 conceptual model (A) and Electrical Image (B). Note: the weathering (intermediate conductivity) zone comes up from under the image depth indicative of a vertical discontinuity; also, the siltstone bedding plane at 291 causes the weathering zone to jut to the left along the discontinuity indicating a preferential horizon

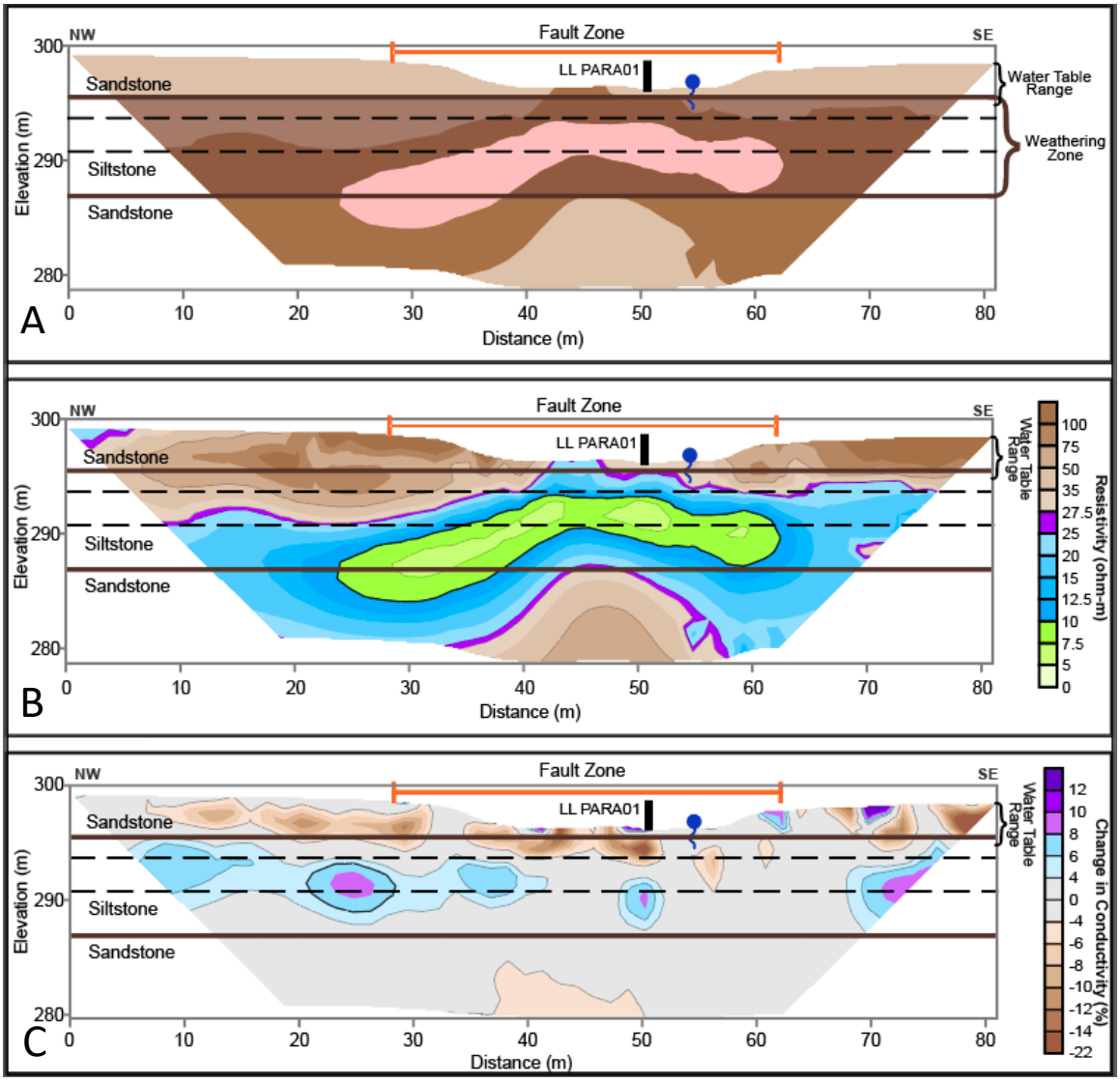

Figure 5. 5 ERI Line LL ORTHO02 conceptual model (A) and Electrical Image (B) and temporal image (C). Note: Here the weathering zone dips down into the hypothesized sandstone layering. A topographic high in the sandstone is seen at the bottom of the image. In the temporal image the bedding plane at 291 m coincides with the locations of conductivity change.

5.3 Hydrologic Data

Barometrically corrected measurements of water level transducer data were plotted on a scatter graph displaying water table elevation vs elapsed times (06/19 – 09/19) for data collected at both the hand dug well and the lake (Figure 5.6). Water table elevation data shows storm events through the study period, however, electrical conductivity and temperature data were only collected for the dates after 8/23/19 (Figure 5.6A). During the storm event noted on 06/06/2019 the water table within the hand dug well rose three meters while the same storm pulse into the lake water caused a lake level increase of less than one meter. Throughout the study storm pulses caused a greater fluctuation of the water table in the hand dug well than the water level of the lake. This is evidence of the slow draining of the aquifer and the fault into the lake.

The hydraulic gradient associated with the difference in water levels at the time of data collection demonstrates how the gradient varied during high and low flow periods (Figure 5.6B). Hydraulic gradient values ranged from 0.089 – 0.116 depending on how much precipitation was received by the aquifer. Electrical conductivity, temperature, and water level fluctuations during the study period shows that during rain events (or water level rise) electrical conductivity of the fluid decreases almost simultaneously while temperature rises then slowly decreases. This demonstrates freshwater infiltration during times of water table rise. All together a total of four rain events occurred during the data collection period (Figure 5.7). A comparison of water level against temperature demonstrates that as the water level rises the temperature begins to spike and then decreases similar to a decay function (Figure 5.7). Electrical conductivity behaves in an opposite way decreasing once the water level rises (Figure 5.7B). Also, right before the

water level rise, we notice a spike in electrical conductivity of 50-150 μS/cm (Figure 5.7B).

The second derivative of the water level recession curve demonstrated the decrease in fluid discharge out of the aquifer immediately after the largest storm event which occurred on 06/06/19 when 56 mm of rainfall occurred (Figure 5.8). The largest discharge from the aquifer resulted within the first day after the storm. Groundwater began draining from the aquifer at a rapid rate about 33.4 m/d^2. Drainage from the aquifer decelerated to 0.0334 m/d^2 a day after the storm. At 16 days after the storm, the drainage rate decreased to 0.0197 m/d^2. At the end of the 44-day period, the aquifer decelerated to a drainage rate of 0.0076 m/d^2. From 1 day after the storm to day 44, the water elevation within the sampling well remained within two meters of the storm peak height (298.6 - 296.7 m amsl).

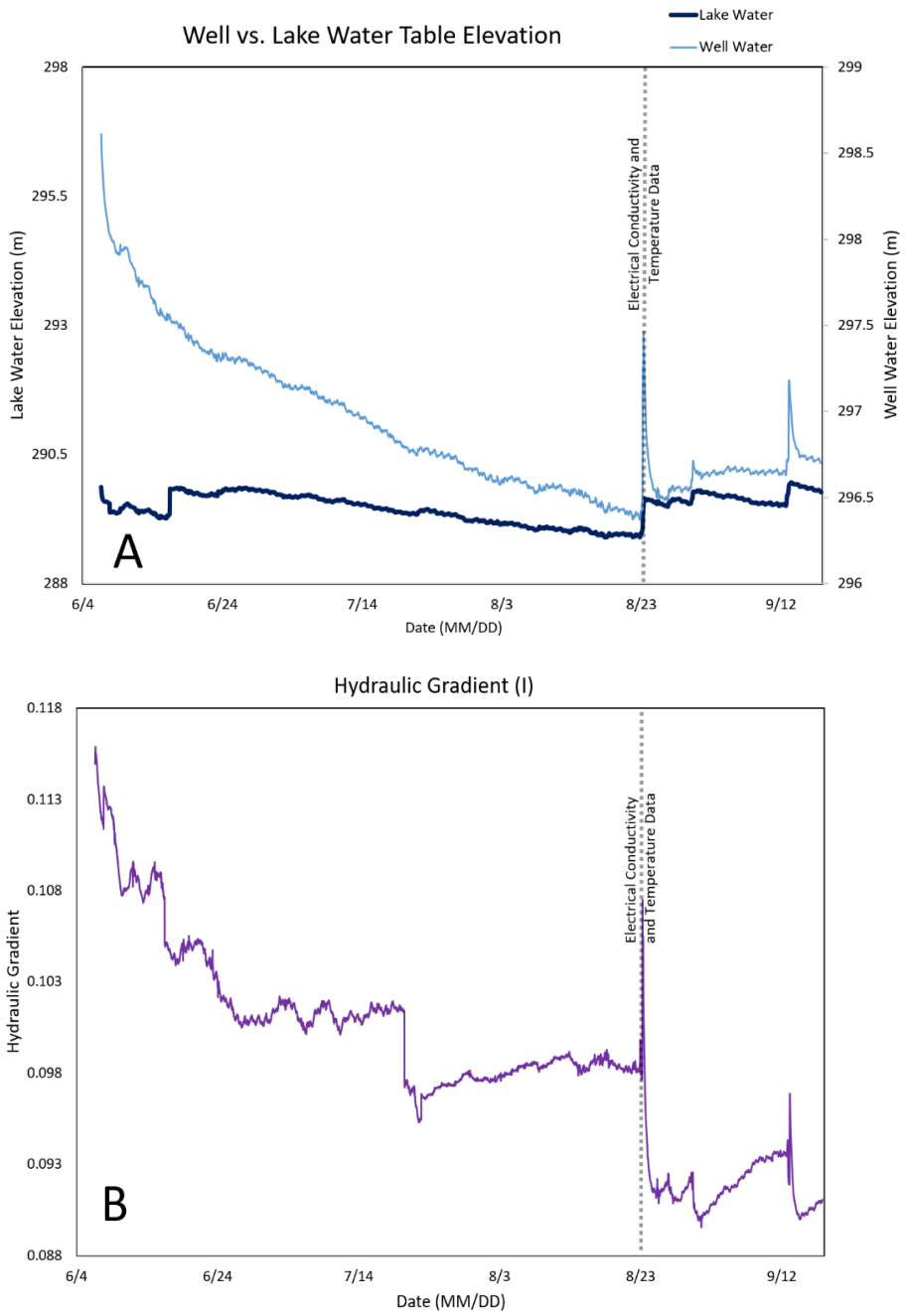

Figure 5. 6 A) Water level elevation from the hand dug well and the dock pressure transducers. B) Hydraulic gradient calculations from the well and dock transducers. Data collected for conductivity and temperature delineation collected after dotted line.

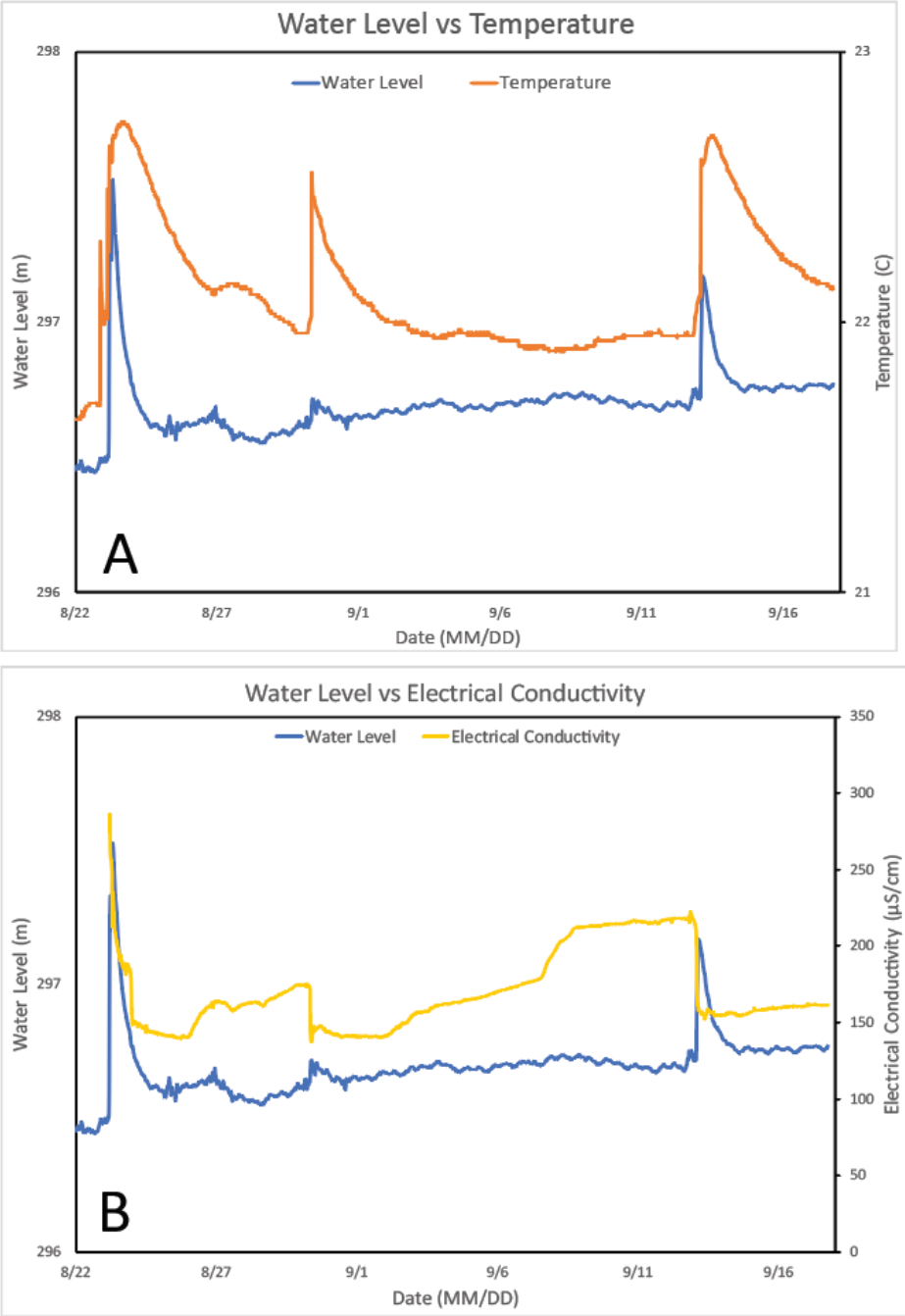

Figure 5. 7 A) A graph of water Level vs temperature. Notice that before the storm pulse arrives the water temperature gets warmer. B) A graph of water level vs electrical conductivity. Notice that as water level rises fluids begin to become less conductive, but before the pulse arrives the conductivity first spikes.

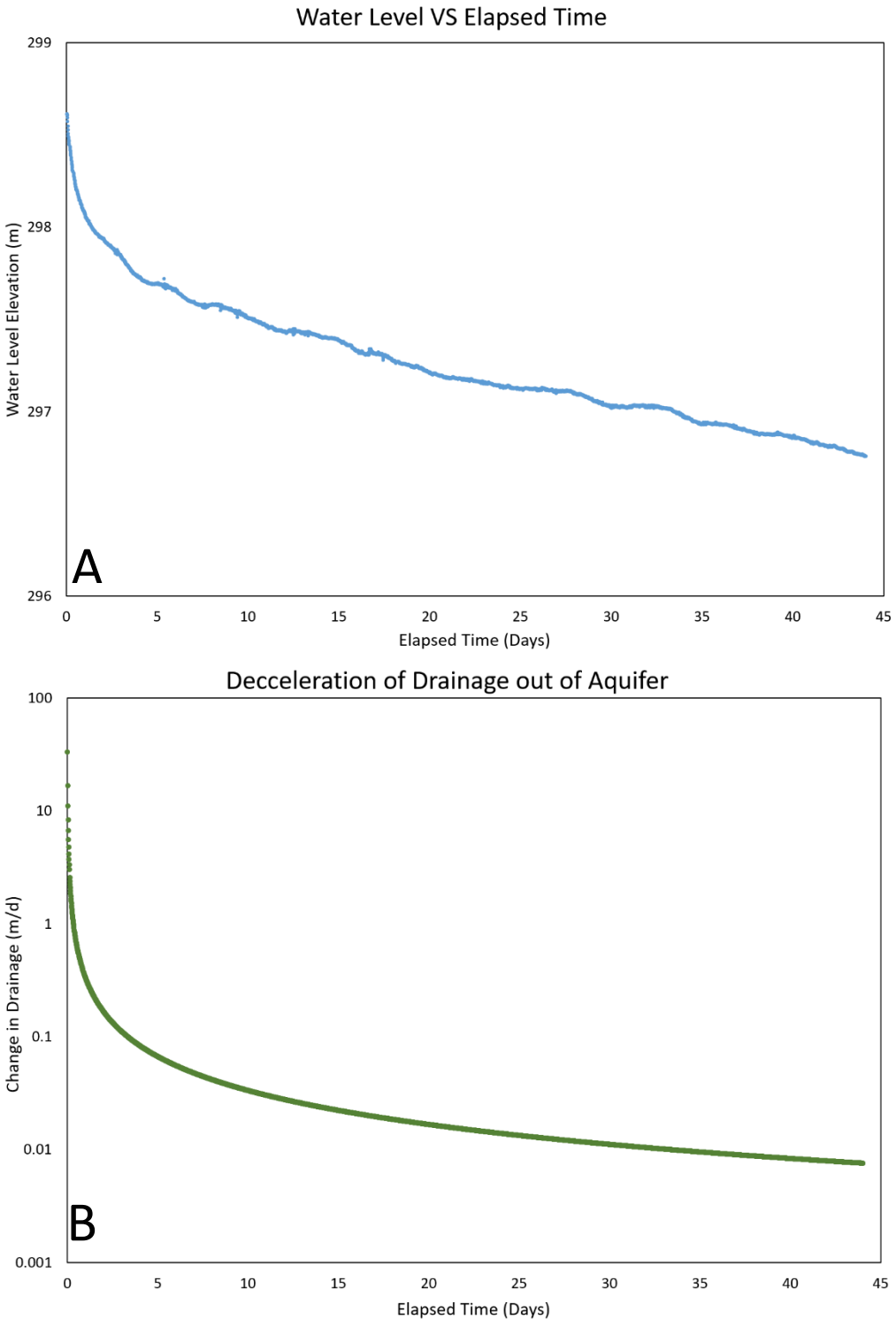

Figure 5.8 Water level vs elapsed time and drainage out of aquifer for the storm period of 06/06/2019-08/23/2019.

5.4 Lithological Data

Hydraulic conductivities quantified from the permeameter produced values ranging from 4.33E-1 m/s to 1.55E-5 m/s. The large range of these values resulted from the methods used to collect the undisturbed sample. In total five samples were collected. Four out of five samples displayed some disturbance on the surface of the sample that reduced the volume of the material available to transport the fluids through the sample. This may have resulted in the large discrepancies between calculated hydraulic conductivities. In the end only one sample lithology was deemed truly undisturbed and was used to hypothesize the hydraulic conductivity of the siltstone matrix. The hydraulic conductivity value quantified from the permeameter was 1.55E-5 m/s.

CHAPTER VI

6.0 DISCUSSION

The development of sandstone pseudokarst requires two primary factors, the release of grains from the matrix and piping of the grains out of the aquifer. At the field site, low permeability stratigraphic horizons restrict the flow of groundwater to preferential pathways along faults or bedding planes that become conduits for piping during storm events. The identification of piping pathways through the collection of land survey, electrical resistivity, and hydrologic datasets allowed for the identification of characteristics required for piping within the aquifer. Mapping and hydrologic data provided evidence to limit lateral flow due to clay deposits on the slope face. In this section we discuss the data to synthesize if groundwater migration through the aquifer results in piping and the quantification of pseudokarst conduits.

6.2 Does Piping Exist at the Field Site?

Studies describing the transport of fluids through sandstones and karst observed that subsurface erosion resulted from the self-organization of flow regimes along preferential pathways (Nieber and Sidle, 2010). These studies delineated that during storm events, fluid migration through buildup of pressure within pore spaces causes the

propagation of the wetting front into lower pressured locations. Along hillslopes this increase of pressure results in a maximum hydraulic gradient along the hillslope face, and causes the reorganization of flow into preferential pathways (Nieber and Sidle, 2010). Nieber and Sidle (2010) concluded that hillslope faces were the area's most susceptible to seepage erosion and piping. An examination of the ERI line LL PARA01 demonstrates that the electrically conductive, low permeability, dry clay zone reaches beneath the hillslope area (Figure 5.3). If we assume the low permeability-clay zone to be a no flow zone relative to the remainder of the aquifer and well mapped as a 10 ohm-m or less deposit, the hydraulic gradient at the base of the hillslope would be 0.34 during the period of maximum hydraulic flux. Bruthans et al. (2012) delineated that a hydraulic gradient value of 0.005 - 0.02 is needed to be achieved in order for piping erosion of a conduit to occur. Throughout our study period the maximum value of hydraulic gradient has been nearly doubled, supporting piping as a mechanism at this site.

Nieber and Sidle (2010) also arrived at the same conclusion that as hydraulic head increases so does sediment discharge, however they concluded that hydraulic gradient wasn't as important of a factor as aquifer structures and seepage paths along conduits (Nieber and Sidle, 2010). The above factors influence both the location of piping and the magnitude/maintenance of the conduits ability to pipe sediment from the aquifer. Aquifer structures like bedding planes and fractures, provide migrating fluids with discontinuities that ultimately become preferential pathways. The sandstone-siltstone interfaces are located at 296 and 287 m, while the bedding planes located at 294 m and 291 m are within the siltstone layer. Discharging water was observed at the upper siltstone bedding plane 294 m in the hand dug well, while fluid flow along the lower siltstone 291 m

bedding plane was delineated from the temporal ERI (figure 4.5). Beneath the lower siltstone 291 m bedding plane, the interface between resistive and less resistive sediment is hypothesized, to be the siltstone – sandstone interface at 287 m. The current data does not identify the presence of an additional flow path at this depth. Conceptual models presented in the previous section identify the hypothesized weathering zones as representing resistivity between 10-25 ohm-m. Fluid propagation through the aquifer is facilitated in the horizontal direction along bedding planes within the siltstone horizon. These bedding planes act as both physical and lithological inception horizons as they focus flow while maintaining the conduit integrity (Bernatek-Jakiel et al., 2020; Filipponi et al., 2009; Marco and Pierre-Yves, 2008; Nadal-Romero et al., 2011). The cohesive siltstone lithology maintains the conduit diameter permitting the continual enlargement of the conduit without the subsidence of the overlying topography. If piping occurred in a less cohesive lithology, like sandstone, subsurface mass removal would cause the simultaneous subsidence of topography overlying the conduit, resulting in a depression similar to a subsidence sinkhole in karst aquifers (Ford and Williams, 2013). Instead, when the conduit is developed in a cohesive lithology, like siltstone, the structure overlying the conduit is maintained, preventing the subsidence of sediment until the conduit becomes too large to hold the overlying sediment. This can be likened to a cover-collapse sinkhole in a karst aquifer (Ford and Williams, 2013). Conduits developed in cohesive sediments allow the continual migration of fluids along the pathway, resulting in longer periods of mass removal. Without conduit development in cohesive sediments, the formation of pseudokarst structures through the aquifer would be limited to landscapes resulting from short lived piping events (Bernatek-Jakiel et al., 2020;

Bernatek-Jakiel and Poesen, 2018; Halliday, 2007; Nieber and Sidle, 2010; Wilson et al., 2018).

The importance of the weathering zone placement lies in siltstone's ability to hold open a conduit to allow the piping of sediments. Commonly pseuokarst are represented as short lived structures only lasting from one storm to the next, due to their inability to maintain a continual pathway for physical erosion (Halliday, 2007). Normally, flow through seepage paths surrounded by coarse (sand) sized grains become restricted by collapsed/blocked pathways often causing the divergence of the conduit into a different pathway forming discontinuous gullies (Anderson et al., 2009; Bruthans et al., 2012; Nadal-Romero et al., 2011; Nieber and Sidle, 2010). To illustrate the susceptibility to collapse, Bruthans et al. (2012) noted that even with a hydraulic gradient greater than 0.7 applied to a block of sandstone with a blocked conduit outlet, for 260 hours, no more than 5% of the blocks volume was eroded, however, when that same block was flooded with fluids the rock was disintegrated within minutes to few hours. This means that the aquifers susceptibility to piping depends on how well the conduit resists collapse when saturated with fluids during times of high hydraulic gradients. If the conduit is blocked but able to maintain some conduit flow, sediments can be transported through the available pore spaces within the conduit. Back-flooding then occurs as a result of the conduit size decrease resulting in an increase of flow velocity, hydraulic gradient, and mass wasting along the flow path (Bruthans et al., 2012; Halihan et al., 1999; Nieber and Sidle, 2010). The pinhole test experiment conducted by Nadal-Romero et al. (2011) indicated that only the silt and clay grain size stratigraphy is stable enough under saturated conditions to maintain an open conduit. They concluded that the piping was

more susceptible in silts than clays due to the cohesiveness of clays being harder to erode into conduits. Bernatek-Jakiel et al. (2020) demonstrated that sediments with clay percentages less than 40% were harder to erode than those with less than 24% clay particles. In sediments with silt representing greater than 50% and clays less than 24%, piping was observed. Silt's degree of cohesion allows piping to occur while preventing the conduit from collapsing. Development of the weathering zone within the relatively stable siltstone lithology appears to generate a continuous conduit capability for this pseudokarst site. Siltstone lithology provide additional stability for the conduits allowing sediments to be released from the conduit walls while still preventing collapse of the overall conduit and the transports of sediments from shallower parts of the stratigraphy.

6.3 Influence of the Subsurface Clay Zone

Sandstone, siltstone, and clays are descriptions of grain sizes within the sedimentary aquifer rather than compositional descriptions of minerals the aquifer contains. The spatial complexities contained in sandstones or siltstones may vary differently according to the initial depositional environment and how the aquifer has responded to various diagenetic processes. At the site, resistivity values between 5-10 ohm-m are hypothesized to represent clay sediment. This hypothesis has been verified by the extraction of gully sediment, during the installation of the dry piezometer. Comparatively, resistivity values between 5 – 100 ohm-m have also been defined as representing clay sized particles in other studies (Palacky, 1987).

The low permeability clay causes lithological heterogeneity within the siltstone leading to constricted flow along the preferential flow path, ultimately resulting in the long term development of conduits along the siltstone bedding planes. The low

permeability clay layer only exists within the siltstone boundary discussed in the previous section. Bedding planes in the siltstone boundary permit fluids to migrate through the aquifer, however the most rapid vertical pathway is likely the vertical faults in the area. Due to the low permeability clay zone that exists in the weathering area on the slope of the site in the fault zone, fluids can enter the fault-controlled gully area but a limited in their ability to discharge from that zone. This results in the initial rapid infiltration of fluids producing large hydraulic gradients and velocities that permit the piping of sediments while the slow drainage of the aquifer allows chemically aggressive waters time for any thermodynamically stable reactions (Figure 5.8). The decrease in drainage rate can be observed in Figure 5.8 while the aggressiveness of fluids infiltrating the aquifer can be observed in Figure 5.7. The low permeability clay zone is of pivotal importance when it comes to the formation of pseudokarst structures at the site, but the clay zone is not extensive throughout the entire site, therefore a question of possible origin must be discussed (Figure 5.3,5.4,5.5).

One possibility for the origin of the clays may be from the defragmentation of sand and silt sized framework grains (Meunier et al., 2007). As most geologic formations contain various compositions of framework grains, dissolved minerals may release ions that can be re-precipitated as authigenic clays (Dutta and Suttner, 1986). This may result in the alteration of the aquifers initial permeability and water saturation throughout the aquifers geologic lifetime (Wilson et al., 1977). The formation of authigenic clays primarily removes porosity by filling in available spaces left from the dissolution of soluble materials and/or the initial deposition of sediment. The data available for this

study does not make it clear whether the clays is a weathering residual of the aquifer, or also includes clay transported through the pseudokarst conduit system.

Data collected from the temporal ERI demonstrated the extent of groundwater migration along the bedding plane at 291m (Figure 5.5-bottom) compared with the rest of the formation. The data indicated that during storm events it was possible for fluids to permeate three meters vertically into the surrounding aquifer. When these data are compared to the ERI image LL ORTHO02 in figure 5.5B the three-meter deep zone reaches into the overlying resistive and underlying conductive sediment. Potentially, during periods of high hydraulic gradients chemically aggressive fluids may discharge out of a conduit and migrate into the siltstone layers providing less weathered rock with chemically aggressive fluids. If this is the case, the dissolution of framework grains within the siltstone layers may release ions that migrate and precipitate authigenic clays when environmental conditions are right. The continual dissolution and precipitation of authigenic clays can lead to the creation of clay lenses. These lenses create micropores that hold fluids irreducibly due to the physical attraction of the liquid to the solid (Velde, 1995). As a result, only under intense gradients can fluids be moved into or out of the clay lens (Kohno, 2020; Neuzil, 1986). Large gradients observed at the site as well as temporal data suggest that during storm events fluids are discharged into the clay medium, providing even more chemically aggressive source of fluids for the continuation of dissolution and precipitation processes occurring within the clay lenses. Pore waters between the authigenic clay particles often contain dissolved molecules, ions, and organic molecules that become exchanged and/or sorbed onto the surfaces of clay sized grains (Velde, 1995). Ions and organic molecules that are sorbed onto clay particles provide

microbial populations with substrate, water, and nutrients necessary for their growth (Atekwana et al., 2006). When provided with the necessary tools the microbial community can develop biofilms in available pore spaces that can further reduce permeability of a lithologic medium 100-500 fold (Proto et al., 2016). Although, this study does not directly prove the microbial degradation of the aquifer, it provides an explanation of the potential location of growth (located in the low permeability zone) and the source of nutrients (located within the preferential pathways) for microbial production. Although the microbial degradation of carbonate rocks is known to contribute to karst landscapes, the role of microbial activity in regards to pseudokarst formation is still poorly understood (Wray and Sauro, 2017).

The constriction caused by the low permeability-clay on the surface of the slope causes the high hydraulic gradient and results in numerous sinkholes throughout the site. Both the slope and the presence of sinkholes ends downslope closer to the lake. We considered this change in slope as the lateral transition on the slope face from siltstone to clay. *Figure 4.2* is an interpretation of this transition zone where the slope reaches the lake. The sinkholes can be observed here existing on the periphery of the siltstone-sandstone transition zone. Table Mountains in Venezuela contained sinkholes that were also were developed along the periphery of the mountain structure (Wray and Sauro, 2017). This was hypothesized to occur as the result of the gravitational release causing the enlargement of joints and fractures along the edge (Wray and Sauro, 2017). Coupled with the mechanical removal of sediment grains, the developed joints and fractures could help to further pipe surface sediment into the subsurface enlarging the surface sinkholes.

Data from the ERI survey coupled with the land survey data provides a partial image of a clay filled gully that extends throughout the sloping section of the site. We hypothesize that this clay filled area restricts flow from protruding through the slope causing water pressure to build up and leading to the discharge of fluids at trinity point and the Garber Ridge Spring. The pressure builds up also cause an increase in linear velocity within the conduit beneath the low permeability zone, inducing piping along the flow paths on the sides of the subsurface clay deposit. Without this low permeability zone, fluids would be expected to discharge from the base of the gully at a velocity still high enough for what it needed for piping. Thus, the subsurface is interpreted as slowing down the pseudokarst process, not accelerating it.

CHAPTER VII

7.0 CONCLUSION

The common conceptual model for pseudokarst development in sandstones parallels the karst conceptual model for carbonate aquifers. Aggressive groundwater migrating through the sandstone dissolves the cement and the ions are migrated along an inception horizon generally at the base of the formation. This field study evaluated the migration timing of aggressive waters and the gradients and pathways to allow piping of largely insoluble grains. Mapping results, combined with temporal water level and EC data, as well as temporal electrical imaging were applied to the field site. The results indicate that fine grain material control the amount of time fluid remains in the aquifer and the location of pseudokarst feature development. The results also indicate that for the study site, the major piping locations are along bedding planes in the interior of an underlying siltstone formation, not at the base of the sandstone that is weathering (Figure 5.5).

The results suggest that while fluid can enter the system rapidly through recharge with fast changes in the water table, the fine materials on the slopes of erosional surfaces can allow fluids to remain in contact with the subsurface for long periods. Chemical evaluation of the weathering periods would be useful to understand what conditions can

cause weathering to increase in these settings. The results also suggest that piping controls due to piping collapse may govern the development of pseudokarst. As the literature suggest that piping in sand is prone to collapse and that clay may be too cohesive for simple pipe development (Bernatek-Jakiel et al., 2020; Nadal-Romero et al., 2011), the role of silt needs to be further investigated. The results of this study suggest an optimal amount of clay or silt will generate the most stable pipes for the subsurface migration of grains out of a pseudokarst formation.

REFERENCES

Aksu, I., et al., 2015, Swelling of clay minerals in unconsolidated porous media and its impact on permeability: GeoResJ, v. 7, p. 1-13.

Aley, T. J., et al., 2012, Down but not straight down: significance of lateral flow in the vadose zone of karst terrains: Carbonates and Evaporites, v. 27, no. 2, p. 193-198.

Ali, M., et al., 2011, Effects of hydraulic parameters on sediment capacity in overland flow over erodible channels: Hydrology and Earth System Sciences Discussions, v. 8, p. 6939-6965.

Anderson, A., et al., 2009, Dye staining and excavation of a lateral preferential flow network: Hydrology & Earth System Sciences, v. 13, no. 6.

Atekwana, E. A., et al., BIOGEOPHYSICS: THE EFFECTS OF MICROBIAL PROCESSES ON GEOPHYSICAL PROPERTIES OF THE SHALLOW SUBSURFACE, Dordrecht, 2006, Springer Netherlands, p. 161-193.

Aubrecht, R., 2012, Venezuelan tepuis : their caves and biota, Comenius University.

Aubrecht, R., et al., 2011, Sandstone caves on Venezuelan tepuis: Return to pseudokarst?: Geomorphology, v. 132, no. 3, p. 351-365.

Bandstra, J. Z., et al., 2008, Compilation of mineral dissolution rates: Kinetics of Water-Rock Interaction, p. 737-824.

Barbel-Périneau, A., et al., 2019, Karst flow processes explored through analysis of long-term unsaturated-zone discharge hydrochemistry: a 10-year study in Rustrel, France: Hydrogeology Journal, v. 27, no. 5, p. 1711-1723.

Bernatek-Jakiel, A., et al., 2020, Sediment detachment in piping-prone soils: Cohesion sources and potential weakening mechanisms: Earth Surface Processes and Landforms, v. 45, no. 13, p. 3185-3201.

Bernatek-Jakiel, A., et al., 2018, Subsurface erosion by soil piping: significance and research needs: Earth-Science Reviews, v. 185, p. 1107-1128.

Bin, L., et al., 2008, Effect of microbial weathering on carbonate rocks: Earth Science Frontiers, v. 15, no. 6, p. 90-99.

Breit, G. N., et al., 1990, Mineralogy and petrography of Permian rocks in the Central Oklahoma aquifer: US Geological Survey Open-File Report, p. 90-678.

Bruthans, J., et al., 2012, Fast evolving conduits in clay-bonded sandstone: Characterization, erosion processes and significance for the origin of sandstone landforms: Geomorphology, v. 177, p. 178-193.

Burley, S., et al., 1986, Thin section and SEM textural criteria for the recognition of cement-dissolution porosity in sandstones: Sedimentology, v. 33, no. 4, p. 587-604.
Carr, J. E., et al., 1977, A preliminary appraisal of the Garber-Wellington Aquifer, southern Logan and northern Oklahoma counties, Oklahoma, 77-278.
Chakraborty, R., et al., 2012, Systems biology approach to bioremediation: Curr Opin Biotechnol, v. 23, no. 3, p. 483-490.
Che-Alota, V., et al., 2009, Temporal geophysical signatures from contaminant-mass remediation: Geophysics, v. 74, no. 4, p. B113-B123.
Clemens, T., et al., 1999, Simulation of the development of karst aquifers: role of the epikarst: International Journal of Earth Sciences, v. 88, no. 1, p. 157-162.
Datta, P., et al., 1996, Major ion chemistry of groundwater in Delhi area: chemical weathering processes and groundwater flow regime: Journal-Geological Society of India, v. 47, p. 179-188.
Doerr, S. H., 1999, Karst-like landforms and hydrology in quartzites of the Venezuelan Guyana shield: Pseudokarst or 'real' karst?: Zeitschrift fur Geomorphologie, v. 43, p. 1-17.
Dreybrodt, W., 1980, Kinetics of the dissolution of calcite and its applications to karstification: Chemical Geology, v. 31, p. 245-269.
Dreybrodt, W., 1990a, A model of Karstification in the vicinity of hydraulic structures: IAHS PUBLICATION, p. 33-33.
Dreybrodt, W., 1990b, The Role of Dissolution Kinetics in the Development of Karst Aquifers in Limestone: A Model Simulation of Karst Evolution: The Journal of Geology, v. 98, no. 5, p. 639-655.
Dubois, C., et al., 2014, The process of ghost-rock karstification and its role in the formation of cave systems: Earth-Science Reviews, v. 131, p. 116-148.
Dutta, P. K., et al., 1986, Alluvial sandstone composition and paleoclimate; II, Authigenic mineralogy: Journal of Sedimentary Research, v. 56, no. 3, p. 346-358.
Eijkelkamp, 2013, 09.02 Laboratory-Permeameters Volume 2021: Eijkelkamp.com, Eijkelkamp.
Filipponi, M., et al., 2009, Evidence of inception horizons in karst conduit networks: Geomorphology, v. 106, no. 1, p. 86-99.
Florea, L. J., et al., 2006, Springflow hydrographs: eogenetic vs. telogenetic karst: Groundwater, v. 44, no. 3, p. 352-361.
Ford, D., et al., 2013, Karst hydrogeology and geomorphology, John Wiley & Sons.
Ghoshal, K., et al., 2014, Grain-size distribution in suspension over a sand-gravel bed in open channel flow: International Journal of Sediment Research, v. 29, no. 2, p. 184-194.
Gibbs, R. J., 1970, Mechanisms controlling world water chemistry: Science, v. 170, no. 3962, p. 1088-1090.
Gjettermann, B., et al., 1997, Preferential flow in sandy loam soils as affected by irrigation intensity: Soil Technology, v. 11, no. 2, p. 139-152.
Glaister, R., et al., 1974, Grain-size distributions, an aid in facies identification: Bulletin of Canadian Petroleum Geology, v. 22, no. 3, p. 203-240.

Graham, C. B., et al., 2010, Hillslope threshold response to rainfall: (1) A field based forensic approach: Journal of Hydrology, v. 393, no. 1, p. 65-76.
Greer, B. M., et al., 2017, Electrical resistivity imaging of hydrologic flow through surface coal mine valley fills with comparison to other landforms: Hydrological Processes, v. 31, no. 12, p. 2244-2260.
Halihan, T., et al., 1999, Interpreting flow using permeability at multiple scales: Karst modeling: Karst Waters Institute Special Publication, v. 5, p. 82-96.
Halihan, T., et al., 1998a, Modeling of storm responses in conduit flow aquifers with reservoirs: Journal of Hydrology, v. 208, no. 1, p. 82-91.
Halihan, T., et al., 1998b, Physical response of a karst drainage basin to flood pulses: example of the Devil's Icebox cave system (Missouri, USA): Journal of Hydrology, v. 204, no. 1, p. 24-36.
Halliday, W. R., 2007, Pseudokarst in the 21st century: Journal of Cave and Karst Studies, v. 69, no. 1, p. 103-113.
Hartkamp, C. A., et al., 1993, Grain size, composition, porosity and permeability contrasts within cross-bedded sandstones in Tertiary fluvial deposits, central Spain: Sedimentology, v. 40, no. 4, p. 787-799.
Hem, J. D., 1985, Study and interpretation of the chemical characteristics of natural water, Department of the Interior, US Geological Survey.
Herman, E. K., et al., 2012, Clastic sediment transport and storage in fluviokarst aquifers: an essential component of karst hydrogeology: Carbonates and Evaporites, v. 27, no. 3, p. 211-241.
Hussain, Y., et al., 2020, The potential use of geophysical methods to identify cavities, sinkholes and pathways for water infiltration: Water, v. 12, no. 8, p. 2289.
Ismail, A., et al., 2012, 2-D and 3-D resistivity imaging of karst sites in Missouri, USA: Environmental & Engineering Geoscience, v. 18, no. 3, p. 281-293.
Jennings, J., 1983, Sandstone pseudokarst or karst: Aspects of Australian Sandstone Landscapes. Australian and New Zealand Geomorphology Group Special Publication, v. 1, p. 21-30.
Kästner, M., et al., 2010, In Situ Microcosm Studies to Characterize Microbial Processes in the Field, *in* Timmis, K. N., ed., Handbook of Hydrocarbon and Lipid Microbiology: Berlin, Heidelberg, Springer Berlin Heidelberg, p. 3503-3511.
Katz, B. G., et al., 1998, Changes in the isotopic and chemical composition of ground water resulting from a recharge pulse from a sinking stream: Journal of Hydrology, v. 211, no. 1, p. 178-207.
Klimchouk, A., et al., 2000, Lithologic and structural controls of dissolutional cave development: Speleogenesis, Evolution of Karst Aquifers, AB Klimchouk, DC Ford, AN Palmer, W. Dreybrodt,(Eds.), National Speleological Society, Huntsville, Alabama, p. 45-53.
Kohno, M., 2020, Effects of Hydraulic Gradient and Clay Type on Permeability of Clay Mineral Materials: Minerals, v. 10, no. 12, p. 1064.
Kovács, A., 2003, Geometry and hydraulic parameters of karst aquifers: a hydrodynamic modeling approach: Université de Neuchâtel.
Kovács, A., et al., 2015, Well hydrograph analysis for the characterisation of flow dynamics and conduit network geometry in a karst aquifer, Bükk Mountains, Hungary: Journal of Hydrology, v. 530, p. 484-499.

Kovács, A., et al., 2008, Modelling karst hydrodynamics: Frontiers of Karst Research, p. 13-26.
Li, X., et al., 2020, Hydraulic Conductivity Behaviors of Karst Aquifer With Conduit-Fissure Geomaterials: Frontiers in Earth Science, v. 8, no. 30.
Marco, F., et al., What makes a bedding plane favourable to karstification?–The role of the primary rock permeability, *in* Proceedings Proceeding of 4th European Speleological Congress–Vercors2008, Citeseer, p. 32.
Martin, J. B., et al., 1999, Temperature as a natural tracer of short residence times for groundwater in karst aquifers: Karst Modeling. Karst Waters Institute Special Publication, v. 5, p. 236-242.
-, 2001, Exchange of water between conduits and matrix in the Floridan aquifer: Chemical Geology, v. 179, no. 1-4, p. 145-165.
Martin, J. M., et al., 2006, Monitoring well responses to karst conduit head fluctuations: Implications for fluid exchange and matrix transmissivity in the Floridan aquifer: Geological Society of America Special Papers, v. 404, p. 209-217.
Martini, J. E., 1979, Karst in black reef quartzite near Kaapsehoop, Eastern Transvaal.
-, 1982, Karst in Black Reef and Wolkberg group quartzite of the easterus Transvaal escarpment South Africa: Boletín de la Sociedad Venezolana de Espeleología, v. 10, no. 19, p. 99-114.
McBride, E. F., 1989, Quartz cement in sandstones: a review: Earth-Science Reviews, v. 26, no. 1-3, p. 69-112.
Mecchia, M., et al., 1999, Hydrogeology and SiO2 geochemistry of the Aonda Cave system (Auyantepui, Bolivar, Venezuela): Boletin Sociedad Venezolana de Espeleologia, v. 33, p. 1-11.
Mecchia, M., et al., 2019, A hybrid model to evaluate subsurface chemical weathering and fracture karstification in quartz sandstone: Journal of Hydrology, v. 572, p. 745-760.
Meeder, J. F., et al., 2019, Origin and development of true karst valleys in response to late Holocene sea-level change, the Transverse Glades of southeast Florida, USA: The Depositional Record, v. 5, no. 3, p. 558-577.
Meng, X., et al., 2016, Arsenic solubilization and redistribution under anoxic conditions in three aquifer sediments from a basin-fill aquifer in Northern Utah: The role of natural organic carbon and carbonate minerals: Applied Geochemistry, v. 66, p. 250-263.
Meunier, A., et al., 2007, The petrography of weathering processes: facts and outlooks: Clay Minerals, v. 42, no. 4, p. 415-435.
Moore, P. J., et al., 2010, Conduit enlargement in an eogenetic karst aquifer: Journal of Hydrology, v. 393, no. 3-4, p. 143-155.
Nadal-Romero, E., et al., 2011, Quantitative assessment of the piping erosion susceptibility of loess-derived soil horizons using the pinhole test: Geomorphology, v. 135, no. 1, p. 66-79.
Neuzil, C. E., 1986, Groundwater flow in low-permeability environments: water resources research, v. 22, no. 8, p. 1163-1195.
Nieber, J. L., et al., 2010, How do disconnected macropores in sloping soils facilitate preferential flow?: Hydrological Processes, v. 24, no. 12, p. 1582-1594.

Onac, B. P., et al., 2011, Minerogenetic mechanisms occurring in the cave environment: an overview: International Journal of Speleology, v. 40, no. 2, p. 79.
Palacky, G., 1987, Clay mapping using electromagnetic methods: First Break, v. 5, no. 8.
Palandri, J. L., et al., 2004, A compilation of rate parameters of water-mineral interaction kinetics for application to geochemical modeling: Geological Survey Menlo Park CA.
Peng, Z., et al., 2016, Understanding the rapidity of subsurface storm flow response from a fracture-oriented shallow vadose through a new perspective: Journal of Hydrology, v. 544.
Piccini, L., et al., 2009, Solution weathering rate and origin of karst landforms and caves in the quartzite of Auyan-tepui (Gran Sabana, Venezuela): Geomorphology, v. 106, no. 1, p. 15-25.
Price, J. R., et al., 2003, Chemical weathering indices applied to weathering profiles developed on heterogeneous felsic metamorphic parent rocks: Chemical geology, v. 202, no. 3-4, p. 397-416.
Proto, C., et al., 2016, Biomediated permeability reduction of saturated sands: Journal of Geotechnical and Geoenvironmental Engineering, v. 142, no. 12, p. 04016073.
Ramakrishna, A., 2011, Characterization of Karst Terrain Using Electrical Resistivity Imaging Technique, Geo-Frontiers 2011: Advances in Geotechnical Engineering, p. 2514-2523.
Rayner, S. F., et al., 2007, Constraining aquifer architecture with electrical resistivity imaging in a fractured hydrogeological setting: Journal of Environmental & Engineering Geophysics, v. 12, no. 4, p. 323-335.
Robinet, J.-C., et al., 2008, The effect of rock matrix heterogeneities near fracture walls on the residence time distribution (RTD) of solutes: Transport in Porous Media, v. 72, no. 3, p. 393-408.
Sauck, W. A., A conceptual model for the geoelectrical response of LNAPL plumes in granular sediments, *in* Proceedings 11th EEGS Symposium on the Application of Geophysics to Engineering and Environmental Problems1998, European Association of Geoscientists & Engineers, p. cp-203-00084.
Sauro, F., 2014, Structural and lithological guidance on speleogenesis in quartz–sandstone: Evidence of the arenisation process: Geomorphology, v. 226, p. 106-123.
Screaton, E., et al., 2004, Conduit Properties and Karstification in the Unconfined Floridan Aquifer: Groundwater, v. 42, no. 3, p. 338-346.
Shanmugam, G., et al., 1988, Porosity enhancement from chert dissolution beneath Neocomian unconformity: Ivishak formation, North Slope, Alaska: AAPG bulletin, v. 72, no. 5, p. 523-535.
Siebert, R., et al., 1984, A theory of framework grain dissolution in sandstones: Part 2. Aspects of Porosity Modification.
Stoeber, M. W., 2005, Minimum Velocities for the Suspension of Fine Sediment in the Green River Canal.
Thullner, M., et al., 2009, Characterization and quantification of in situ biodegradation of groundwater contaminants using stable isotope fractionation analysis: advantages and limitations, p. 41-81.

Utom, A. U., et al., 2019, Adaptive observation-based subsurface conceptual site modeling framework combining interdisciplinary methodologies: a case study on advancing the understanding of a groundwater nitrate plume occurrence: Environmental Science and Pollution Research, v. 26, no. 16, p. 15754-15766.
Vacher, H. L., et al., 2002, Eogenetic karst from the perspective of an equivalent porous medium: Carbonates and Evaporites, v. 17, no. 2, p. 182-196.
Velde, B., 1995, Composition and mineralogy of clay minerals, Origin and mineralogy of clays, Springer, p. 8-42.
Vesper, D. J., et al., 2004, Storm pulse chemographs of saturation index and carbon dioxide pressure: implications for shifting recharge sources during storm events in the karst aquifer at Fort Campbell, Kentucky/Tennessee, USA: Hydrogeology Journal, v. 12, no. 2, p. 135-143.
Viollier, E., et al., 2000, The ferrozine method revisited: Fe(II)/Fe(III) determination in natural waters: Applied Geochemistry, v. 15, no. 6, p. 785-790.
Walker, T. R., et al., 1978, Diagenesis in first-cycle desert alluvium of Cenozoic age, southwestern United States and northwestern Mexico: Geological Society of America Bulletin, v. 89, no. 1, p. 19-32.
White, W. B., 2002, Karst hydrology: recent developments and open questions: Engineering Geology, v. 65, no. 2, p. 85-105.
White, W. B., et al., 1995, Karst lands: American scientist, v. 83, no. 5, p. 450-459.
Williams, P. W., 1983, The role of the subcutaneous zone in karst hydrology: Journal of Hydrology, v. 61, no. 1, p. 45-67.
Wilson, G. V., et al., 2013, Pore-Water Pressures Associated with Clogging of Soil Pipes: Numerical Analysis of Laboratory Experiments: Soil Science Society of America Journal, v. 77, no. 4, p. 1168-1181.
Wilson, G. V., et al., 2016, Soil pipe flow tracer experiments: 1. Connectivity and transport characteristics: Soil Pipe Flow Tracer Experiments: Hydrological processes, v. 30, no. 8, p. 1265-1279.
Wilson, G. V., et al., 2018, Sediment detachment and transport processes associated with internal erosion of soil pipes: Earth Surface Processes and Landforms, v. 43, no. 1, p. 45-63.
Wilson, M. D., et al., 1977, Authigenic clays in sandstones; recognition and influence on reservoir properties and paleoenvironmental analysis: Journal of Sedimentary Research, v. 47, no. 1, p. 3-31.
Worden, R., et al., 2003, Sandstone diagenesis: the evolution of sand to stone: Sandstone diagenesis: Recent and ancient, v. 4, p. 3-44.
Worden, R., et al., 1998, Carbonate cement in the Triassic Chaunoy Formation of the Paris Basin: distribution and effect on flow properties: Carbonate cementation in sandstones: distribution patterns and geochemical evolution, p. 163-177.
Worthington, S. H., et al., Porosity and permeability enhancement in unconfined carbonate aquifers as a result of dissolution, *in* Proceedings SPELEO Brazil 2001-13th International Congress of Speleology2001.
Worthington, S. R. H., 2015, Characteristics of channel networks in unconfined carbonate aquifers: GSA Bulletin, v. 127, no. 5-6, p. 759-769.

Wray, R. A. L., 2009, Phreatic drainage conduits within quartz sandstone: Evidence from the Jurassic Precipice Sandstone, Carnarvon Range, Queensland, Australia: Geomorphology, v. 110, no. 3, p. 203-211.

Wray, R. A. L., et al., 2017, An updated global review of solutional weathering processes and forms in quartz sandstones and quartzites: Earth-Science Reviews, v. 171, p. 520-557.

Zhu, C., 2005, In situ feldspar dissolution rates in an aquifer: Geochimica et Cosmochimica Acta, v. 69, no. 6, p. 1435-1453.

VITA

Jordon Patrick Massey

Candidate for the Degree of

Master of Science

Thesis: HYDROLOGICAL CONTROLS ON PSEUDOKARST IN A PERMIAN SANDSTONE SILTSTONE AQUIFER, OKLAHOMA

Major Field: Geology

Biographical:

Born and raised in Detroit, Michigan on October 27th, 1994 to Hubert W Massey and Marquitta J. Massey.

Education:

Completed the requirements for the Master of Science in Geology at Oklahoma State University, Stillwater, Oklahoma in December, 2021.

Completed the requirements for the Bachelor of Science in Geology at Western Michigan University, Kalamazoo, MI, USA in 2021.

Experience:

Graduate Teaching Assistant, Boone Pickens School of Geology, Oklahoma State University, January 2019 to December 2019

Experience: Graduate Teaching Assistant, Boone Pickens School of Geology, Oklahoma State University, January 2020 to December 2021